ELSEVIER

J. Non-Newtonian Fluid Mech. 125 (2005) 121–141

Journal of Non-Newtonian Fluid Mechanics

www.elsevier.com/locate/jnnfm

Instability of high-frequency modes in viscoelastic plane Couette flow past a deformable wall at low and finite Reynolds number

A. Sameer Kumar, V. Shankar*

Department of Chemical Engineering, Indian Institute of Technology, Kanpur 208016, India

Received 31 May 2004; received in revised form 27 September 2004; accepted 27 September 2004

Abstract

The linear stability of plane Couette flow of an upper convected Maxwell (UCM) fluid of viscosity η, density ρ, relaxation time τ_R and thickness R flowing past a linear viscoelastic solid of shear modulus G and thickness HR is analyzed using a combination of asymptotic analysis (at low Reynolds number) and numerical solution (at finite Reynolds number). The asymptotic analysis is used to analyze the effect of wall deformability on a class of high frequency modes in the UCM fluid with $c \sim O(Re^{-1/2})$ at $Re \ll 1$ first studied by Gorodtsov and Leonov [J. Appl. Math. Mech. 31 (1967) 310–319; abbreviated GL here], who showed that these modes are stable in a rigid channel. Here, c is the wavespeed of perturbations (nondimensionalised by V), $Re = \rho VR/\eta$ is the Reynolds number, V is the velocity of the moving plate. Our asymptotic results show that *all* the high frequency–low Re modes of GL are rendered unstable by solid wall deformability. The variation of the growth rate with the nondimensional solid elasticity parameter $\Gamma = V\eta/(GR)$ shows an oscillatory behavior alternating between stable and unstable regions, and the variation for upstream traveling waves is completely antiphase with that for downstream waves. The parameter Γ is shown to be proportional to $Re^{1/4}$ at $Re \ll 1$ for neutrally stable downstream waves. Numerical continuation shows that the instability at low Re continues to finite Re, and typically the instability ceases to exist above a critical Re. This critical Re increases with an increase in the Weissenberg number $W = \tau_R V/R$. In some cases, however, the instability continues to very high Re, and $\Gamma \propto Re^{-1}$ in that limit for neutrally stable modes. Neutral stability curves in the Γ–W plane show that the predicted instability of the high frequency GL modes exists only at finite and large W, and is absent in the Newtonian fluid ($W \to 0$) limit. The asymptotic analysis for the Oldroyd-B model shows that the ratio of solvent viscosity to total viscosity of the solution should be $O(Re^{1/2})$ in order for the instability to exist at low Re, meaning the instability is absent for realistic values of solvent viscosity at low Re. However, numerical results show that the instability of the high-frequency GL modes is present at finite Re in an Oldroyd-B fluid, and increasing solvent viscosity ratio has a stabilizing effect on the instability. Similarly, the solid to fluid viscosity ratio η_r also has a stabilizing effect at finite Re, but in the limit of low Re, $\eta_r \sim O(Re^{1/2})$ in order for the instability to exist. Our study thus demonstrates the presence of an instability in viscoelastic plane Couette flow past a deformable wall which is primarily due to the viscoelastic nature of the fluid, and is absent in Newtonian fluids.

Keywords: Viscoelastic fluids; Deformable solids; Linear stability analysis; Interfacial instability

1. Introduction

The study of stability of fluid flow past soft, deformable solid surfaces is relevant to a diverse class of applications such as flow in biological systems, polymer processing, and more recently, in microfluidic devices [1,2]. The shear modulus of soft solids is typically in the range 10^3–10^6 Pa, and such soft solids are easily deformed by moderate fluid stresses, which leads to a coupling of the dynamics of the fluid flow with the deformation in the solid wall. A clear understanding of the instabilities that occur in flow past deformable solid media, and the way in which the solid affects these instabilities will help in the accurate design and development of these applications. The linear stability of *Newtonian* fluid flow past deformable solids has been extensively studied in the recent past [3–9], and these studies have shown that novel instabilities exist in flow past deformable solid media that are *absent* in flow past rigid surfaces. However, there are many instances in which the fluid could be viscoelastic: many bio-

* Corresponding author. Tel.: +91 512 259 7377.
E-mail address: vshankar@iitk.ac.in (V. Shankar).

0377-0257/$ – see front matter © 2004 Elsevier B.V. All rights reserved.
doi:10.1016/j.jnnfm.2004.09.010

Nomenclature

$c = c_r + ic_i$ complex wave-speed
G shear modulus of the solid
H nondimensional thickness of the wall
k wavenumber
R dimensional thickness of fluid
$Re = RV\rho/\eta$ Reynolds number of the flow
V dimensional velocity of the top plate
$W = \tau_R V/R$ Weissenberg number

Greek letters

β ratio of solvent to total viscosity in the Oldroyd-B fluid
$\Gamma = V\eta/(GR)$ nondimensional solid elasticity parameter
η viscosity of the fluid
$\eta_r = \eta_w/\eta$ ratio of wall to fluid viscosity
η_w viscosity of the deformable solid wall
τ_R relaxation time in the UCM model

logical fluids are non-Newtonian in nature and could exhibit viscoelastic behavior, and polymer solutions and melts are, of course, viscoelastic fluids. From a practical viewpoint, one might envisage the use of deformable solid surfaces to induce instabilities at low Reynolds number, and the resulting flows may provide a novel way of promoting mixing in viscoelastic fluids. From a fundamental standpoint, a pertinent question is whether viscoelastic effects can induce additional modes of instabilities apart from those existent in Newtonian flow past deformable solid media. A first step in this direction was taken by Shankar and Kumar [10] who studied the stability of viscoelastic plane Couette flow past a deformable solid in the creeping flow limit, but the instability they found was a continuation of the already existent instability in Newtonian fluids modified by fluid viscoelastic effects. In this study, we use both asymptotic and numerical methods to analyze the effect of wall deformability on a class of high frequency modes first studied by Gorodtsov and Leonov [11] for plane Couette flow of upper convected Maxwell fluid in a rigid channel. We predict here a new instability in viscoelastic plane Couette flow past a deformable wall that is absent in Newtonian fluids. In the following discussion, we briefly recapitulate relevant previous literature, and motivate the context for the present study.

Gorodtsov and Leonov [11] (abbreviated as GL in this paper) first analyzed the stability of plane Couette flow of an upper convected Maxwell (abbreviated UCM hereafter) fluid in rigid channels. GL essentially analyzed two types of modes: (1) In Section 2 of their paper, they neglected the inertial terms in the fluid and considered the creeping flow limit (Reynolds number $Re = 0$), where they showed that there are two stable discrete eigenvalues for the wavespeed. In this paper, we refer to these two discrete eigenvalues as 'zero Reynolds number GL modes', and this is henceforth abbreviated as ZRGL modes. (There also exists a continuous spectrum of eigenvalues [12], which are always stable, and we restrict our discussion only to the discrete part of the spectrum.) (2) In Section 3 of their paper, GL analyzed the stability problem in the $Re \ll 1$ limit, but with wave speed $c \sim Re^{-1/2} \gg 1$ (if the Weissenberg number $W \sim O(1)$). This corresponds to very high frequency of oscillations of the perturbations in the limit of low Re. In this limit, some of the inertial terms in the governing stability equation for the fluid cannot be neglected despite the $Re \ll 1$ limit. GL carried out an asymptotic analysis in the small parameter $Re^{1/2}$ and calculated the wavespeed as an asymptotic series. Their results show that there are *multiple solutions* to the leading order wavespeed, all of which are real. Consequently, the first correction to the wavespeed determines the stability of the system, which they demonstrate to be stable for all the solutions. These results are valid in the limit $Re \ll 1$. We refer to these solutions as the 'high frequency GL modes', and this is abbreviated as HFGL in the following discussion. Physically, for perturbations at high frequencies (compared to the shear rate of the base Couette flow), the UCM fluid behaves similar to an elastic solid, and the HFGL modes in a UCM fluid are essentially identical to shear waves in an elastic solid [13]. The wavespeed of shear waves in an elastic solid is proportional to $\sqrt{G/\rho}$ where G is the shear modulus of the solid and ρ is the density. If we estimate the elastic modulus of the UCM fluid (with viscosity η, relaxation time τ_R and density ρ) as $\sqrt{\eta/\tau_R}$, then the dimensional shear wave speed for a UCM fluid is proportional to $\sqrt{\eta/(\tau_R\rho)}$. Upon nondimensionalising this wavespeed with the velocity V in the Couette flow, one obtains the nondimensional wavespeed as $c \propto Re^{-1/2}W^{-1/2}$ for elastic shear waves, which is the scaling assumed by GL in their analysis. Therefore, the discrete solutions to c obtained by GL in their high-frequency analysis are elastic shear waves in a UCM fluid modified by the presence of the Couette flow. Apart from these two class of modes, they also carry out (in Section 4 of their paper) an asymptotic analysis in the limit $kW \gg 1$, and conclude *incorrectly* (proved subsequently by Renardy and Renardy [14]) that the UCM plane Couette flow is unstable in this limit.

Subsequent numerical analysis using a spectral method by Renardy and Renardy [14] showed that the UCM plane Couette flow is always stable at finite Re, and they reported a set of discrete eigenvalues from their spectral method. In Section 3 of this paper, we show that these numerically computed discrete spectrum of eigenvalues are nothing but a continuation of the HFGL modes (discussed above) and the two ZRGL modes to finite Re. Renardy [15] further proved rigorously that the UCM plane Couette flow is *stable* at $Re = 0$, and for arbitrary values of W. Similarly, Sureshkumar and Beris [16] showed using a numerical method that the viscoelastic plane Poiseuille flow of a UCM fluid is also stable at $Re = 0$ for all W. The earlier study of Ho and Denn [17] analyzed

the stability of plane Poiseuille flow of an UCM fluid in rigid channels using a numerical shooting procedure, and showed that the flow is stable at low *Re* and finite *W*. Wilson et al. [12] studied the spectrum for UCM and Oldroyd-B fluids at $Re = 0$ in both plane Couette and combined Couette-plane Poiseuille configurations. They showed how the discrete spectrum changes as the Couette flow is changed to a plane Poiseuille flow and also as the constitutive model is changed from UCM to Oldroyd-B fluid. All these previous studies, however, analyzed the stability of viscoelastic flow in rigid channels.

Shankar and Kumar [10] recently studied the effect of wall deformability on the two ZRGL modes in the creeping flow limit, where the inertial effects in the fluid and the solid were neglected. At fixed Weissenberg number *W*, they showed that one of the two discrete stable ZRGL modes becomes unstable upon increase of the nondimensional solid elasticity parameter $\Gamma = V\eta/(GR)$ above a critical value. However, when neutral stability curves were constructed in the Γ–*W* plane, they found that this unstable mode continues to the limit of $W \to 0$ (Newtonian fluid), and in this limit, it reduces to the Newtonian fluid instability past a deformable wall first studied by Kumaran et al. [3]. Thus, the continuation of the stable ZRGL modes to finite wall deformability gives the same unstable mode as the continuation of the unstable mode of Kumaran et al. to finite Weissenberg number. Therefore, the effect of wall deformability on the ZRGL modes does not give rise to a qualitatively new instability, rather it is just a modification of the instability existing in Newtonian fluids by fluid viscoelastic effects. The elastic nature of the UCM fluid has a stabilizing effect on the Newtonian fluid instability, and the instability ceases to exist in the UCM fluid when the nondimensional group $\tau_R G/\eta$ is greater than a certain critical value.

The effect of wall deformability on the stability of the HFGL class of solutions studied by GL [11], however, has not been analyzed, and this is the subject of the present study. For the HFGL class of modes, $c \sim Re^{-1/2}$ in the limit of low *Re*, so inertial effects in the fluid come into play even in the $Re \ll 1$ limit. One might similarly expect the inertial effects in the deformable solid also to become important for this class of modes. In the absence of flow, both the UCM fluid and the elastic solid will admit elastic shear waves, which are stable due to viscous effects in the fluid. The presence of the plane Couette flow in the fluid will modify these shear waves, and we analyze how the flow affects the stability of the shear waves when the fluid flows past an elastic solid. To this end, we first use an asymptotic analysis in the $Re \ll 1$, $W \sim \mathrm{O}(1)$ limit to examine the effect of wall deformability on the HFGL modes, and we continue these results to finite *Re* using a numerical method. In terms of the 'elasticity number' $E \equiv W/Re$ often used to characterize viscoelastic flows [16], our asymptotic analysis corresponds to the limit of $E \gg 1$, and the small parameter of our asymptotic analysis is $E^{-1/2}$. The numerical results extend the asymptotic results at $E \gg 1$ to finite values of $E \sim \mathrm{O}(1)$. We also contrast the continuation of the previous zero-*Re* instability of Shankar and Kumar [10] to finite *Re* with the present results.

The primary objective of the present study is to qualitatively demonstrate the presence of a new class of unstable modes in viscoelastic flow past deformable solid surfaces due to the elastic nature of the fluid, and the simple UCM model suffices for this purpose. However, some preliminary numerical results for the Oldroyd-B model (which adds a solvent viscosity contribution to the UCM model) are also presented, in order to show that the predicted instability could be potentially observed even in the presence of nonzero solvent viscosity. Despite the use of these simple models to describe the viscoelastic fluid, it is expected that the present instability should exist even in more realistic models for polymer solutions and melts.

The rest of this paper is organized as follows. In Section 2, we develop the governing linear stability equations and boundary conditions, and also describe and validate the numerical method used to solve the coupled fluid–solid stability equations. In Section 3, we demonstrate that the numerically computed discrete spectrum for UCM plane Couette flow in rigid channels [14] is nothing but a finite-*Re* continuation of the ZRGL and HFGL modes first analyzed by GL. Section 4.1 presents the asymptotic analysis for UCM Couette flow past a deformable wall, and also the results from the analysis in the limit $Re \ll 1$. Section 4.2 provides some representative numerical results at finite *Re* for both the UCM and Oldroyd-B models. Section 5 summarizes the salient results from the present study.

2. Problem formulation and numerical method

2.1. Governing equations

The system of interest consists of a linear viscoelastic solid of thickness *HR* and shear modulus *G* fixed onto a rigid surface at $z^* = -HR$, and a layer of viscoelastic fluid of thickness *R* in the region $0 < z^* < R$ (see Fig. 1). The viscoelastic fluid is modeled using the UCM model (see, for example, [18]), which has two material constants: a constant viscosity η and a relaxation time τ_R. In what follows, we denote dimensional variables with a superscript * and nondimensional variables without any superscript. The fluid is bounded

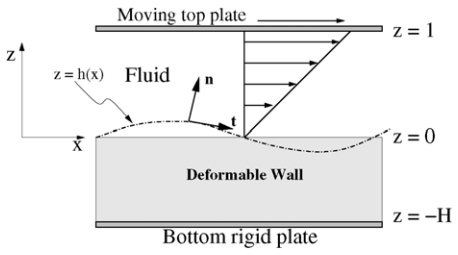

Fig. 1. Schematic diagram showing the configuration and (nondimensional) coordinate system considered in this paper.

at $z^* = R$ by a rigid plate which moves at a constant velocity V in the x-direction relative to the deformable solid wall. The following scales are used for nondimensionalising various quantities at the outset: R for lengths and displacements, V for velocities, R/V for time, and $\eta V/R$ for stresses and pressure. Thus, H is the nondimensional thickness of the deformable solid layer.

The nondimensional equations governing the dynamics of the fluid are the mass and momentum conservation equations:

$$\partial_i v_i = 0, \qquad Re[\partial_t + \partial_j v_j]v_i = \partial_j T_{ij}. \tag{1}$$

Here, v_i is the velocity field in the fluid, $Re = \rho VR/\eta$ is the Reynolds number in the fluid, $T_{ij} = -p_f\delta_{ij} + \tau_{ij}$ is the total stress tensor in the fluid which is a sum of an isotropic pressure $-p_f\delta_{ij}$ and the extra-stress tensor τ_{ij}, and the indices i and j can take the values x, z. The extra-stress tensor is given by the UCM constitutive relation as:

$$W[\partial_t\tau_{ij} + v_k\partial_k\tau_{ij} - \partial_k v_i\tau_{kj} - \partial_k v_j\tau_{ki}] + \tau_{ij} = (\partial_i v_j + \partial_j v_i), \tag{2}$$

where $\partial_t \equiv (\partial/\partial t)$, $\partial_i \equiv (\partial/\partial x_i)$, and $W = \tau_R V/R$ is the Weissenberg number characterizing the relaxation time of the viscoelastic fluid. No-slip conditions are appropriate for the velocity field in the fluid at $z = 1$:

$$v_x = 1, \qquad v_z = 0, \tag{3}$$

while the conditions at the interface between the fluid and the deformable solid wall are discussed below.

The deformable solid wall is modeled as an incompressible linear viscoelastic solid, similar to that used in the previous studies in this area (see, for example, [3,4,10]). Recently, Gkanis and Kumar [19] have examined the consequences of using a nonlinear model for describing the deformation in the solid wall, by using the neo-Hookean model for analyzing the stability of creeping Newtonian flow past a deformable wall. This study has shown that for nonzero interfacial tension and sufficiently large values of H, the results from both linear and nonlinear solid models agree quite well, while for small values of $H < 2$, the linear model somewhat overpredicts the critical velocity required for destabilizing the flow. They also predict a shortwave instability in the absence of interfacial tension at the solid–fluid interface, and this was attributed to the nonzero first normal stress difference in the neo-Hookean solid. In this study, we restrict ourselves to the linear viscoelastic solid model, and it is argued later in this paper that the linear solid model is expected to yield accurate results for the present instability. The deformable solid is described by a displacement field u_i which represents the displacement of the material points from their steady-state positions. The velocity field in the wall medium is $v_i = \partial_t u_i$. The solid medium is assumed to be incompressible, and hence the displacement field satisfies the solenoidal condition:

$$\partial_i u_i = 0. \tag{4}$$

The momentum conservation equation in the solid layer is given by

$$Re\,\partial_t^2 u_i = \partial_j \Pi_{ij}, \tag{5}$$

where $\Pi_{ij} = -p_g\delta_{ij} + \sigma_{ij}$ is the total stress tensor in the solid which is given by a sum of the isotropic pressure $-p_g\delta_{ij}$ and the deviatoric stress tensor σ_{ij}. Without loss of generality, we have set the density of the solid equal to the density of the fluid ρ. The deviatoric stress σ_{ij} is given by a sum of elastic and viscous stresses in the deformable solid:

$$\sigma_{ij} = \left(\frac{1}{\Gamma} + \eta_r\partial_t\right)(\partial_i u_j + \partial_j u_i), \tag{6}$$

where $\Gamma = V\eta/(GR)$ is the nondimensional parameter characterizing the elasticity of the solid layer, and $\eta_r = \eta_w/\eta$ is the ratio of wall to fluid viscosities. The nondimensional group Γ is the estimated ratio of viscous stresses in the fluid to elastic stresses in the solid layer. The solid layer is assumed to be fixed to a rigid surface at $z = -H$, and so the boundary condition there is $u_i = 0$.

The conditions at the interface $z = h(x)$ between the fluid and the deformable solid wall are the continuity of velocities and stresses:

$$v_i = \partial_t u_i, \qquad T_{ij}n_j = \Pi_{ij}n_j, \tag{7}$$

where n_j is the unit normal to the interface $z = h(x)$ (see Fig. 1). The normal and tangential stress continuity conditions at the interface are obtained by contracting the second equation in Eq. (7) with the unit normal and tangent vectors. When the interfacial tension between the fluid and the solid layer is nonzero, additional terms appear in the normal stress continuity.

2.2. Base state

The steady, unidirectional base state velocity profile whose stability is of interest in this study is simply the plane Couette flow profile:

$$\bar{v}_x = z, \qquad \bar{v}_z = 0,$$
$$\bar{\tau}_{xx} = 2W, \qquad \bar{\tau}_{zz} = 0, \qquad \bar{\tau}_{xz} = \bar{\tau}_{zx} = 1. \tag{8}$$

All the base flow quantities are denoted by an overbar here and in the following discussion. Note the presence of a nonzero first normal stress difference $\bar{\tau}_{xx} - \bar{\tau}_{zz} = 2W$ which is absent in the case of Newtonian fluids. The deformable solid wall is at rest in this steady base state, but there is a nonzero unidirectional displacement field $\bar{u}_x$ due to the fluid stresses at the interface:

$$\bar{u}_x = \Gamma(z + H), \qquad \bar{u}_z = 0,$$
$$\bar{\sigma}_{xx} = \bar{\sigma}_{zz} = 0, \qquad \bar{\sigma}_{xz} = \bar{\sigma}_{zx} = 1. \tag{9}$$

The fluid–solid interface is uniform and flat in this base state.

2.3. Linear stability analysis

A temporal linear stability analysis is used to determine the stability of the above base state, where small perturbations (denoted by primed quantities) are introduced to the fluid velocity field about the base state $v_i = \bar{v}_i + v_i'$, and other dynamical quantities in the fluid and the solid are similarly perturbed. The perturbation quantities are expanded in the form of Fourier modes in the x-direction, and with an exponential dependence in time:

$$v_i' = \tilde{v}_i(z)\exp[\mathrm{i}k(x-ct)], \qquad u_i' = \tilde{u}_i(z)\exp[\mathrm{i}k(x-ct)], \tag{10}$$

where k is the wavenumber, c is the complex wavespeed, and $\tilde{v}_i(z)$ and $\tilde{u}_i(z)$ are eigenfunctions which have to be determined from the linearized governing equations and boundary conditions. The complex wavespeed is given by $c = c_\mathrm{r} + \mathrm{i}c_\mathrm{i}$ and when $c_\mathrm{i} > 0$, the base state is temporally unstable.

Upon substituting the above form for the perturbations in the governing equations (1) and the constitutive relation for the UCM fluid (2), we obtain the following linearized governing equations (where $\mathrm{d}_z = \mathrm{d}/\mathrm{d}z$):

$$\mathrm{d}_z\tilde{v}_z + \mathrm{i}k\tilde{v}_x = 0, \tag{11}$$

$$-\mathrm{i}k\tilde{p}_\mathrm{f} + \mathrm{i}k\tilde{\tau}_{xx} + \mathrm{d}_z\tilde{\tau}_{xz} = Re[\mathrm{i}k(z-c)\tilde{v}_x + \tilde{v}_z], \tag{12}$$

$$-\mathrm{d}_z\tilde{p}_\mathrm{f} + \mathrm{d}_z\tilde{\tau}_{zz} + \mathrm{i}k\tilde{\tau}_{xz} = Re[\mathrm{i}k(z-c)\tilde{v}_z], \tag{13}$$

$$\{1 + \mathrm{i}kW(z-c)\}\tilde{\tau}_{zz} = 2\mathrm{d}_z\tilde{v}_z + 2\mathrm{i}kW\tilde{v}_z, \tag{14}$$

$$\{1 + \mathrm{i}kW(z-c)\}\tilde{\tau}_{xz} = (\mathrm{d}_z\tilde{v}_x + \mathrm{i}k\tilde{v}_z) + W(\tilde{\tau}_{zz} + 2\mathrm{i}kW\,\tilde{v}_z), \tag{15}$$

$$\{1 + \mathrm{i}kW(z-c)\}\tilde{\tau}_{xx} = 2\mathrm{i}k\tilde{v}_x + W(2\tilde{\tau}_{xz} + 4\mathrm{i}kW\tilde{v}_x + 2\mathrm{d}_z\tilde{v}_x). \tag{16}$$

Following [11], we obtain a single fourth-order ordinary differential equation (ODE) for $\tilde{v}_z$ from the above equations:

$$\{\xi^2\mathrm{d}_z^2 - 2\xi\mathrm{d}_z + 2 - k^2\xi^2\}\{\mathrm{d}_z^2 + 2\mathrm{i}kW\mathrm{d}_z - k^2(1+2W^2)\}\tilde{v}_z = -k^2W\,Re\,\xi^3(z-c)[\mathrm{d}_z^2 - k^2]\tilde{v}_z, \tag{17}$$

where the variable ξ is defined as $\xi = [z - c - \mathrm{i}/(kW)]$.

The governing equations for the displacement field in the deformable solid wall can be expressed in terms of $\tilde{u}_i(z)$ in a similar manner to give:

$$\mathrm{d}_z\tilde{u}_z + \mathrm{i}k\tilde{u}_x = 0, \tag{18}$$

$$-\mathrm{i}k\tilde{p}_g + \left(\frac{1}{\Gamma} - \mathrm{i}kc\eta_\mathrm{r}\right)(\mathrm{d}_z^2 - k^2)\tilde{u}_x = -Re\,k^2c^2\tilde{u}_x, \tag{19}$$

$$-\mathrm{d}_z\tilde{p}_g + \left(\frac{1}{\Gamma} - \mathrm{i}kc\eta_\mathrm{r}\right)(\mathrm{d}_z^2 - k^2)\tilde{u}_z = -Re\,k^2c^2\tilde{u}_z. \tag{20}$$

These equations can be reduced to a single fourth-order differential equation for $\tilde{u}_z$:

$$(\mathrm{d}_z^2 - k^2)\left[\mathrm{d}_z^2 - k^2\left(1 - \frac{\Gamma Re\,c^2}{1 - \mathrm{i}kc\eta_\mathrm{r}\Gamma}\right)\right]\tilde{u}_z = 0. \tag{21}$$

The linearized boundary conditions at the unperturbed interface position $z = 0$ between the fluid and the solid layer are obtained by Taylor-expanding about the flat interface position in the base state [3,10]:

$$\tilde{v}_z = (-\mathrm{i}kc)\tilde{u}_z, \tag{22}$$

$$\tilde{v}_x + \tilde{u}_z = (-\mathrm{i}kc)\tilde{u}_x, \tag{23}$$

$$-\tilde{p}_\mathrm{f} + \tilde{\tau}_{zz} - \Sigma k^2\tilde{u}_z = -\tilde{p}_g + 2\left(\frac{1}{\Gamma} - \mathrm{i}kc\eta_\mathrm{r}\right)\mathrm{d}_z\tilde{u}_z, \tag{24}$$

$$\tilde{\tau}_{xz} - 2\mathrm{i}kW\tilde{u}_z = \left(\frac{1}{\Gamma} - \mathrm{i}kc\eta_\mathrm{r}\right)(\mathrm{d}_z\tilde{u}_x + \mathrm{i}k\tilde{u}_z). \tag{25}$$

Here, $\Sigma = \gamma/(\eta V)$ is the nondimensional parameter characterizing the interfacial tension (γ) between the fluid and the solid layer. The second term in the left side of Eqs. (23) and (25) represent nontrivial contributions that arise as a result of the Taylor expansion of the mean flow quantities about the unperturbed interface. The term in Eq. (23) arises due to the discontinuity in the gradient of the base flow velocity profile at the interface, while the term in Eq. (25) arises due to the discontinuity of the first normal stress difference between the fluid and the deformable solid. The boundary conditions at $z = 1$ are simply

$$\tilde{v}_z = 0, \qquad \tilde{v}_x = 0, \tag{26}$$

while the boundary conditions at $z = -H$ are

$$\tilde{u}_z = 0, \qquad \tilde{u}_x = 0. \tag{27}$$

The two fourth order differential equations (17) and (21) for $\tilde{v}_z$ and $\tilde{u}_z$ along with the eight interface and boundary conditions (Eqs. (22)–(27)) completely specify the linear stability problem. The complex wavespeed c is a function of Re, W, Γ, η_r, k, Σ and H. For arbitrary values of Re, there is no closed form solution to the fourth order Eq. (17), and so a numerical method must be used to solve the stability problem in general.

2.3.1. Linear stability equations for Oldroyd-B fluid

In this section, we present the linear stability equations for an Oldroyd-B fluid of total viscosity η, and solvent viscosity $\beta\eta$, where β is the ratio of solvent viscosity to total viscosity of the polymer solution. The nondimensional scales are similar to those used for the UCM fluid in the preceding discussion, with η taking the meaning of the total fluid viscosity. The extra-stress tensor $\tilde{\tau}_{ij}$ is comprised of the Newtonian solvent part and the polymer part: $\tilde{\tau}_{ij} = \tilde{\tau}_{ij}^\mathrm{s} + \tilde{\tau}_{ij}^\mathrm{p}$. The linearized momentum equations and the constitutive relations for the Oldroyd-B fluid are given by:

$$\mathrm{d}_z\tilde{v}_z + \mathrm{i}k\tilde{v}_x = 0, \tag{28}$$

$$Re[\mathrm{i}k(z-c)\tilde{v}_x + \tilde{v}_z] = -\mathrm{i}k\tilde{p}_\mathrm{f} + \beta(\mathrm{d}_z^2 - k^2)\tilde{v}_x + \mathrm{i}k\tilde{\tau}_{xx}^\mathrm{p} + \mathrm{d}_z\tilde{\tau}_{xz}^\mathrm{p}, \quad (29)$$

$$Re[\mathrm{i}k(z-c)\tilde{v}_z] = -\mathrm{d}_z\tilde{p}_\mathrm{f} + \beta(\mathrm{d}_z^2 - k^2)\tilde{v}_z + \mathrm{d}_z\tilde{\tau}_{zz}^\mathrm{p} + \mathrm{i}k\tilde{\tau}_{xz}^\mathrm{p}, \quad (30)$$

$$\{1 + \mathrm{i}kW(z-c)\}\tilde{\tau}_{zz}^\mathrm{p} = 2(1-\beta)\mathrm{d}_z\tilde{v}_z + 2\mathrm{i}kW(1-\beta)\tilde{v}_z, \quad (31)$$

$$\{1 + \mathrm{i}kW(z-c)\}\tilde{\tau}_{xz}^\mathrm{p} = (1-\beta)[\mathrm{d}_z\tilde{v}_x + \mathrm{i}k\tilde{v}_z + 2W^2\mathrm{i}k\,\tilde{v}_z] + W\tilde{\tau}_{zz}^\mathrm{p}, \quad (32)$$

$$\{1 + \mathrm{i}kW(z-c)\}\tilde{\tau}_{xx}^\mathrm{p} = (1-\beta)[2\mathrm{i}k\tilde{v}_x + W(4\mathrm{i}kW\tilde{v}_x + 2\mathrm{d}_z\tilde{v}_x)] + 2W\tilde{\tau}_{xz}^\mathrm{p}. \quad (33)$$

The base state quantities for the Oldroyd-B fluid are identical to that for the UCM fluid (Eq. (8)), except for the normal stress $\bar{\tau}_{xx}$, which is given by $\bar{\tau}_{xx} = 2(1-\beta)W$ for the Oldroyd-B fluid. The boundary conditions at the interface $z = 0$ are identical to those for the UCM fluid (Eqs. (22)–(27)), with the understanding that $\tilde{\tau}_{ij}$ is the sum of polymer and solvent stress in the Oldroyd-B fluid, and the second term in the left side of Eq. (25) acquires a coefficient $(1-\beta)$ due to occurrence of the same factor in $\bar{\tau}_{xx}$ in the Oldroyd-B fluid.

2.4. Numerical method

In this section, we briefly describe and validate the numerical procedure used to solve the stability problem formulated in the previous section. There are two linearly independent solutions to Eq. (17) for $\tilde{v}_z$ consistent with the two boundary conditions at $z = 1$ in the fluid, and two linearly independent solutions to Eq. (21) for $\tilde{u}_z$ consistent with the two boundary conditions at $z = -H$. The numerical method used for determining these linearly independent solutions is a fourth order Runge–Kutta integrator with adaptive step size control along with a Gram–Schmidt orthonormalization procedure, similar to that used in the previous studies for Newtonian fluids [7,9,20]. The eigenfunctions for the fluid velocity field and the solid displacement field are substituted into the four interface conditions (22)–(25) at $z = 0$, and a 4×4 characteristic matrix is obtained. The determinant of this matrix is set to zero to obtain the wavespeed c. A Newton–Raphson iteration technique is then used to obtain the solution.

It is well documented in the literature (see, for example, [14]) that this method is not guaranteed to capture all the eigenvalues of the problem, as this requires a good initial guess to converge to the desired solution. Consequently, a spectral method is often used to compute the eigenvalues of the stability problem in viscoelastic fluids. However, in this study, we use an asymptotic analysis at low *Re* and demonstrate below that this asymptotic (analytical) calculation is guaranteed to yield *all the eigenvalues* in the low *Re* limit. We then use the results from the asymptotic analysis as starting guesses and continue the low *Re* results to finite and intermediate *Re*. In Section 3, we demonstrate this procedure by computing all the eigenvalues given by Renardy and Renardy [14], who employed a spectral method for the case of UCM plane Couette flow in a rigid channel.

Table 1
Validation of numerical method: comparison of present results with that of Renardy and Renardy [14] for UCM plane Couette flow in a rigid channel

Present results		Renardy and Renardy	
c_r	c_i	c_r	c_i
±0.646223	−4.968632	±0.6462	−4.9687
±6.337042713	−2.531036373	±6.3370	−2.5311
±9.831459367	−2.494893485	±9.8315	−2.4949
±13.725512853	−2.506282141	±13.726	−2.5063
±17.155370329	−2.497060553	±17.155	−2.4971
±20.861262474	−2.502570976	±20.861	−2.5026
±24.299596674	−2.498343463	±24.300	−2.4984
±27.940157556	−2.501391939	±27.940	−2.5014
±31.389267116	−2.498952979	±31.389	−2.4999
±34.997086404	−2.500868795	±34.997	−2.5009

Data for $W = 0.2$, $Re = 1$, $k = 1$, and the fluid domain is in the region $z = -1$ to 1.

Three tests were carried out to validate our numerical method and computer code. First, we validated the numerical scheme for the fluid part of the problem by calculating the eigenvalues for UCM plane Couette flow in a rigid channel. For this purpose, we used the numerical results of Renardy and Renardy [14] as starting guesses and we computed the eigenvalues from our procedure. In order to facilitate exact comparison with Renardy and Renardy's results, the fluid domain was changed to $z = -1$ to $z = 1$, with the bottom plate moving in the $-x$ direction with a (nondimensional) velocity 1 which was used in their work. Tables 1 and 2 show some representative comparisons of the eigenvalues obtained from our numerical method with those of Renardy and Renardy.

Table 2
Validation of numerical method: comparison of present results with that of Renardy and Renardy [14] for UCM plane Couette flow in a rigid channel

Present results		Renardy & Renardy	
c_r	c_i	c_r	c_i
±0.774013	−0.369843	±0.7740	−0.36985
±2.186246352	−0.345816106	±2.1862	−0.34582
±3.511632945	−0.279037761	±3.5116	−0.27904
±4.535380249	−0.246776826	±4.5354	−0.24678
±5.682246784	−0.258916137	±5.6822	−0.25892
±6.744561617	−0.246309687	±6.7466	−0.24631
±7.872004491	−0.253954094	±7.8720	−0.25396
±8.950017680	−0.247616371	±8.9500	−0.24762
±10.073418746	−0.252257469	±10.073	−0.25226
±11.159963026	−0.248402701	±11.160	−0.24841

Data for $W = 2$, $Re = 1$, $k = 1$, and the fluid domain is in the region $z = -1$ to 1.

This comparison shows that our results agree very well with the previous results of Renardy and Renardy. It should be noted that there exist solutions [14] with the same imaginary part c_i and with real part c_r having the same magnitude but with opposite signs. Secondly, in order to validate the numerical procedure for the combined fluid–solid problem at finite *Re*, we compared the results obtained from our method for $W \to 0$ with the previous numerical results of Srivatsan and Kumaran [20] who studied the stability of plane Couette flow of a Newtonian fluid, and again excellent agreement was obtained. Thirdly, we also compared the results obtained from our method in the $Re \to 0$ limit, but at finite *W*, with those of Shankar and Kumar [10], who obtained analytical solutions for the stability of UCM Couette flow past a deformable wall in the creeping flow limit, and found very good agreement.

3. Structure of stable modes at low and finite *Re* for UCM plane Couette flow in a rigid channel

In this section, we demonstrate that the eigenvalues of the discrete spectrum for UCM plane Couette flow in rigid channels computed by Renardy and Renardy [14] at $Re \sim O(1)$ are essentially a finite-*Re* continuation of the high frequency–low *Re* and zero *Re* stable modes of Gordotsov and Leonov [11]. GL carried out an asymptotic analysis (see Section 1 of this paper for a brief review of GL's analysis) in the small parameter $Re^{1/2}$ and calculated the wavespeed as an asymptotic series. If we stipulate that $W \sim O(1)$, GL's asymptotic series takes the form $c = Re^{-1/2}(c^{(0)} + Re^{1/2}\, c^{(1)} + \cdots)$. Their results show that there are multiple solutions to the leading order wavespeed $c^{(0)}$, all of which are real. Consequently, the first correction $c^{(1)}$ determines the stability of the system, which they demonstrate to be stable for all the solutions. These results are valid in the limit $Re \ll 1$, and these solutions are referred to as HFGL modes in this paper. Apart from these high frequency solutions in the low *Re* limit, there are two solutions to the wavespeed for which $c \sim O(1)$ and these are obtained by neglecting the inertial effects in the fluid. These two discrete modes are referred to as the ZRGL modes in this paper. The numerical results of Renardy and Renardy [14] (shown in Tables 1 and 2 in this paper) at finite *Re* show that the first eigenvalue corresponds to the pair of ZRGL modes (with c_r having positive and negative values, and the same c_i). At finite *Re*, they reported a number of other stable discrete eigenvalues computed from their spectral method.

We were interested in examining the evolution of the HFGL modes to finite *Re*, and the connection (if any) between these stable modes and the numerically determined modes of Renardy and Renardy [14] at finite values of *Re*. We repeated GL's high frequency asymptotic analysis and calculated only the leading order wavespeed $c^{(0)}$ using the symbolic package *Mathematica*. We briefly outline the asymptotic analysis in Section 4.1 in the context of the stability of these HFGL modes past a deformable wall. Here, we merely state the results for a rigid channel. In order to facilitate the comparison with the results of Renardy and Renardy, the fluid domain ranges from $z = -1$ to 1, and the bottom rigid plate has a velocity -1. The first correction was not required because the leading order wavespeed was found to be a sufficiently good initial guess for our numerical procedure. The characteristic equation admits multiple solutions to $c^{(0)}$, all of which are real. The first few solutions to the leading order wavespeed obtained from the asymptotic analysis are displayed in Table 3. For ease of discussion, we designate numbers to the various solutions based on increasing magnitude of $c^{(0)}$, i.e., the solution with the lowest magnitude of $c^{(0)}$ is referred to as 'mode 1', and increasing mode numbers are given to solutions with increasing magnitudes of $c^{(0)}$. There exist solutions for $c^{(0)}$ with the same magnitude but with opposite signs, and these two solutions correspond to downstream ($c^{(0)}$ positive) and upstream ($c^{(0)}$ negative) traveling waves in the system. The leading order solutions for $c^{(0)}$ are provided as starting guesses at low *Re* (say $Re = 10^{-4}$) to the numerical procedure described previously, and these solutions are continued to finite *Re*.

Table 3
The first nine modes for the leading order wavespeed $c^{(0)}$ calculated from GL's high frequency asymptotic analysis

$W = 0.2$	$W = 2$
±6.82068	±2.26768
±10.1611	±3.54169
±13.954	±4.5692
±17.3403	±5.69414
±21.0114	±6.75548
±24.4292	±7.87805
±28.0522	±8.95583
±31.4893	±10.0774
±35.0865	±11.1639

Data for $k = 1$, $Re \ll 1$. The fluid domain ranges from $z = -1$ to 1.

The numerical solutions to *c* show that it is a complex quantity, and has a *negative* imaginary part indicating that the flow is stable in this limit for this class of modes. Also, for each mode, there are two solutions corresponding to upstream and downstream traveling waves (having the same magnitude but opposite signs for the real part of *c*), but both these solutions have the same negative c_i value. Figs. 2 and 3 show the evolution of *c* with *Re* for the first few HFGL modes obtained from the asymptotic analysis. Importantly, we find that the continuation of the HFGL solutions for $c^{(0)}$ at low *Re* to $Re = 1$ yields all the numerically found modes in Renardy and Renardy's analysis shown in the first two columns of Tables 1 and 2, except for the very first row in these tables which is a continuation of the ZRGL mode to finite *Re*. Indeed, even without doing the numerical continuation to finite *Re*, it is possible to see the connection by directly comparing the $Re \to 0$ asymptotic result for $c^{(0)}$ in Table 3 with the $Re = 1$ numerical result for c_r in Tables 1 and 2. Since $Re = 1$ (and so $Re^{-1/2} = 1$) in these tables, the asymptotic result for $c^{(0)}$ is in fact the actual real part of the wavespeed predicted by the low *Re* asymptotic analysis.

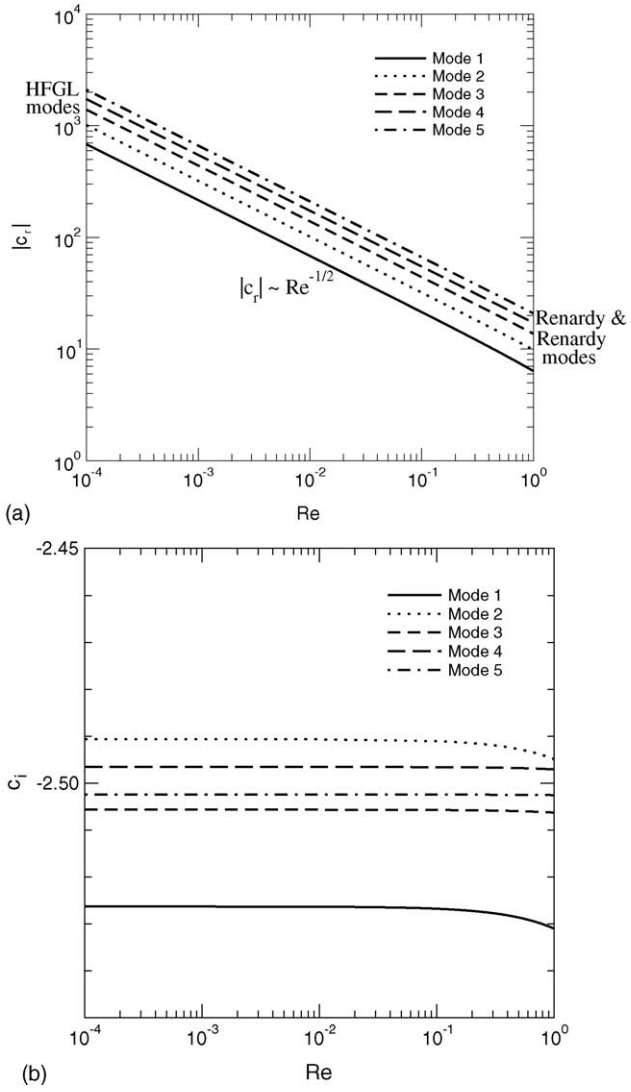

Fig. 2. Continuation of the first few high-frequency GL modes from low *Re* to finite *Re* in a rigid channel. Data for $W = 0.2$, $k = 1$ for the configuration $-1 \le z \le 1$ with the lower rigid plate moving in the opposite direction. (a) c_r vs. *Re*; (b) c_i vs. *Re*.

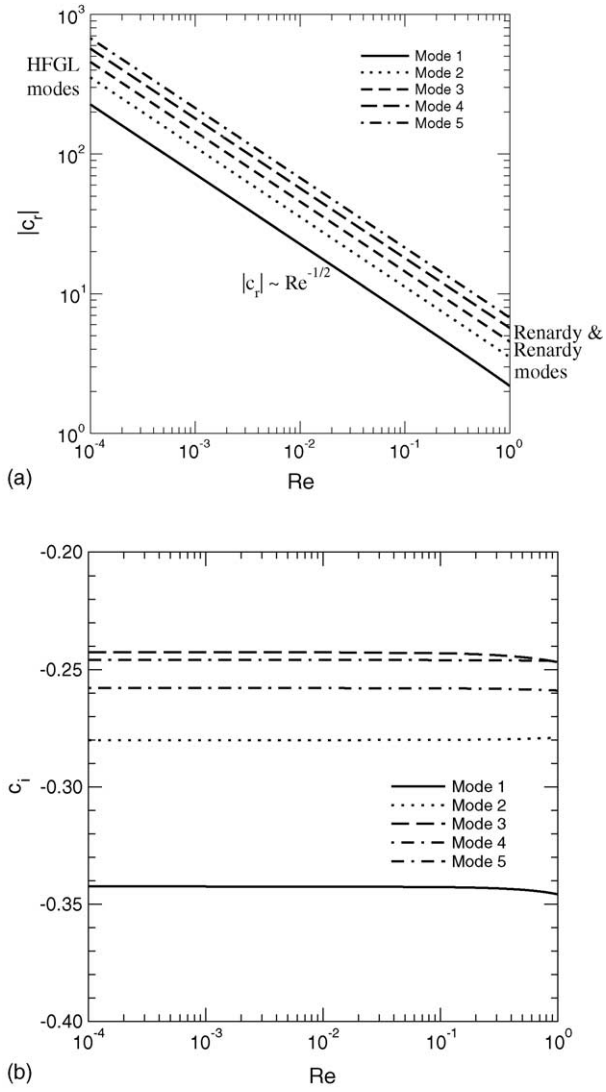

Fig. 3. Continuation of the first few high-frequency GL modes from low *Re* to finite *Re* in a rigid channel. Data for $W = 2$, $k = 1$ for the configuration $-1 \le z \le 1$ with the lower rigid plate moving in the opposite direction. (a) c_r vs. *Re*; (b) c_i vs. *Re*.

The first row in the Tables 1 and 2 correspond to the $Re = 0$ GL (ZRGL) mode, and the real parts of all the rest of the modes in these tables are quite close to the asymptotic results in Table 3, despite the fact that the numerical results are for $Re = 1$. We have also verified that the other set of data for $k = 15$, $W = 1$, $Re = 0.25$ presented in Renardy and Renardy's paper are also a continuation of the high frequency GL modes. Therefore, this comparison suggests that all the stable discrete modes for the UCM plane Couette flow problem at finite *Re* were already present in GL's paper, albeit in the low *Re* limit. To the best of our knowledge, this connection between the ZRGL and HFGL modes at low *Re* and the discrete modes computed numerically at finite *Re* [14] has not been made explicit in the literature on the linear stability of UCM plane Couette flow. With the aid of both the zero *Re* analysis and the low-*Re*, high frequency asymptotic analysis of GL, it is therefore possible to generate *all* the discrete stable modes for UCM plane Couette flow in rigid channels at low *Re*, and the numerical procedure outlined in Section 2.4 can be used to continue these solutions to any desired finite *Re*.

It is useful here to remark on the nature of the modes for UCM Couette flow in a rigid channel if the fluid domain is changed to $0 \le z \le 1$, and if the bottom rigid wall at $z = 0$ is stationary. In that case, the two discrete ZRGL modes have the same c_i (negative) value, but with very different c_r values. For the domain used by Renardy and Renardy [14] where $z = -1$ to $z = 1$, with the bottom plate moving with a velocity -1, the two discrete ZRGL modes have the same negative c_i value and with real part c_r having the same magnitude but opposite signs. For the HFGL class of modes, however, in the domain $z = 0$ to $z = 1$ with the $z = 0$ boundary being stationary, the

numerical solutions show that for each mode there are two solutions with c_r having very nearly the same magnitude (the agreement improves as $Re \ll 1$) and opposite signs, and with the same (negative) value of c_i. For the configuration used by Renardy and Renardy, for each mode there are two solutions with c_r having exactly the same magnitude even at finite Re.

4. Effect of wall deformability on high frequency GL modes

In this section, the effect of wall deformability on the HFGL modes is examined first using an asymptotic analysis in the limit $Re \ll 1$, and then using the numerical procedure described in Section 2.4.

4.1. Asymptotic analysis at low Re

Following Section 3 of GL [11], we consider the limit $Re \ll 1$, and $c \sim Re^{-1/2} \gg 1$. In the original GL analysis, the relevant small parameter was $(Re/W)^{1/2}$. However, in the present analysis, we consider $W \sim O(1)$, and so the appropriate small parameter is simply $Re^{1/2}$. The wavespeed is therefore expanded in an asymptotic series:

$$c = Re^{-1/2}c^{(0)} + c^{(1)} + \cdots. \tag{34}$$

In the present study, further analysis indicates that it is sufficient to calculate only the leading order wavespeed $c^{(0)}$. Upon substituting this expansion in the governing fourth order ODE for the fluid (17), the leading order equation in this limit becomes:

$$\{d_z^2 - k^2\}\{d_z^2 + 2ikWd_z + k^2[(c^{(0)})^2W - 1 - 2W^2]\}\tilde{v}_z = 0. \tag{35}$$

Although $Re \ll 1$, since $c \sim Re^{-1/2}$, the inertial terms in the left side of Eq. (17) contribute the term $k^2(c^{(0)})^2W(d_z^2 - k^2)\tilde{v}_z$ to the above leading order equation. If the velocities in the fluid are expanded in an asymptotic series as:

$$\tilde{v}_z = Re^{-1/2}\,\tilde{v}_z^{(0)} + \tilde{v}_z^{(1)} + \cdots,$$
$$\tilde{v}_x = Re^{-1/2}\,\tilde{v}_x^{(0)} + \tilde{v}_x^{(1)} + \cdots, \tag{36}$$

then the equations governing the stresses in the fluid (Eqs. (14)–(16)) suggest the following expansions for the stresses:

$$\tilde{\tau}_{zz} = \tilde{\tau}_{zz}^{(0)} + Re^{1/2}\,\tilde{\tau}_{zz}^{(1)} + \cdots, \tag{37}$$

$$\tilde{\tau}_{xz} = \tilde{\tau}_{xz}^{(0)} + Re^{1/2}\,\tilde{\tau}_{xz}^{(1)} + \cdots, \tag{38}$$

$$\tilde{\tau}_{xx} = \tilde{\tau}_{xx}^{(0)} + Re^{1/2}\,\tilde{\tau}_{xx}^{(1)} + \cdots. \tag{39}$$

The x–momentum equation in the fluid, Eq. (12), fixes the magnitude of the pressure in the fluid which is expanded as:

$$\tilde{p}_f = \tilde{p}_f^{(0)} + Re^{1/2}\,\tilde{p}_f^{(1)} + \cdots. \tag{40}$$

Upon substituting the above expansions in the Eqs. (12)–(16), we obtain the following simplified expressions for the stresses and the pressure to leading order:

$$-ikWc^{(0)}\tilde{\tau}_{zz}^{(0)} = 2d_z\tilde{v}_z^{(0)} + 2ikW\tilde{v}_z^{(0)}, \tag{41}$$

$$-ikWc^{(0)}\tilde{\tau}_{xz}^{(0)} = (d_z\tilde{v}_z^{(0)} + ik\tilde{v}_z^{(0)}) + 2ikW^2\tilde{v}_z^{(0)}, \tag{42}$$

$$-ikWc^{(0)}\tilde{\tau}_{xx}^{(0)} = 2ik\tilde{v}_x^{(0)} + 4ikW^2\tilde{v}_x^{(0)} + 2Wd_z\tilde{v}_x^{(0)}, \tag{43}$$

$$-ik\tilde{p}_f^{(0)} = -ikc^{(0)}\tilde{v}_x^{(0)} - ik\tilde{\tau}_{xx}^{(0)} - d_z\tilde{\tau}_{xz}^{(0)}. \tag{44}$$

Comparing these simplified leading order equations for $c \sim Re^{-1/2} \gg 1$ with the original set of Eqs. (14)–(16), it is clear that only the 'elastic part' of the left side of these equations manifest in this limit. This is because the high frequency perturbations under consideration here 'probe' only the elastic nature of the viscoelastic fluid to leading order in the analysis.

The velocity continuity conditions (22) and (23) suggest the expansions for the solid displacement field: since $\tilde{v}_z \sim Re^{-1/2}$, $\tilde{u}_z \sim O(1)$ because $c \sim Re^{-1/2}$. Therefore, the displacement and pressure fields in the solid layer are expanded as follows:

$$\tilde{u}_z = \tilde{u}_z^{(0)} + Re^{1/2}\,\tilde{u}_z^{(1)} + \cdots, \tag{45}$$

$$\tilde{u}_x = \tilde{u}_x^{(0)} + Re^{1/2}\,\tilde{u}_x^{(1)} + \cdots, \tag{46}$$

$$\tilde{p}_g = \tilde{p}_g^{(0)} + Re^{1/2}\,\tilde{p}_g^{(1)} + \cdots. \tag{47}$$

Eqs. (19) and (20) reveal that in order for the solid elastic stresses to be of the same order as the solid viscous stresses, the viscosity ratio $\eta_r \sim Re^{1/2} \ll 1$ in the limit of $Re \ll 1$. Therefore, we set $\eta_r = \eta_r^{(0)}Re^{1/2}$ where $\eta_r^{(0)}$ is an O(1) quantity. Upon substituting these expansions in Eqs. (18)–(20), we obtain the following simplified leading order governing equations in the solid medium:

$$d_z\tilde{u}_z^{(0)} + ik\tilde{u}_x^{(0)} = 0, \tag{48}$$

$$-ik\tilde{p}_g^{(0)} + \left(\frac{1}{\Gamma} - ikc^{(0)}\eta_r^{(0)}\right)(d_z^2 - k^2)\tilde{u}_x^{(0)} = -k^2(c^{(0)})^2\tilde{u}_x^{(0)}, \tag{49}$$

$$-d_z\tilde{p}_g^{(0)} + \left(\frac{1}{\Gamma} - ikc^{(0)}\eta_r^{(0)}\right)(d_z^2 - k^2)\tilde{u}_z^{(0)} = -k^2(c^{(0)})^2\tilde{u}_z^{(0)}. \tag{50}$$

Similar to the fluid governing equations, the inertial terms in the solid layer appear at the leading order equations even in the $Re \ll 1$ limit because the term $c^2Re \sim O(1)$ in the right side of Eqs. (19) and (20) due to $c \sim O(Re^{-1/2})$. The above three equations can be combined to give a single fourth order differential equation for the solid layer:

$$(d_z^2 - k^2)\left[d_z^2 - k^2\left(1 - \frac{\Gamma(c^{(0)})^2}{1 - ikc^{(0)}\eta_r^{(0)}\Gamma}\right)\right]\tilde{u}_z^{(0)} = 0. \tag{51}$$

We next turn to the scaling of the interface conditions (Eqs. (22)–(25)) using the above asymptotic expansions. The leading order interface conditions in the limit $Re \ll 1$, $c \sim Re^{-1/2}$ are:

$$\tilde{v}_z^{(0)} = -\mathrm{i}kc^{(0)}\tilde{u}_z^{(0)}, \tag{52}$$

$$\tilde{v}_x^{(0)} = -\mathrm{i}kc^{(0)}\tilde{u}_x^{(0)}, \tag{53}$$

$$\tilde{\tau}_{xz}^{(0)} - 2\mathrm{i}kW\tilde{u}_z^{(0)} = \left(\frac{1}{\Gamma} - \mathrm{i}kc^{(0)}\eta_\mathrm{r}^{(0)}\right)[\mathrm{d}_z\tilde{u}_x^{(0)} + \mathrm{i}k\tilde{u}_z^{(0)}], \tag{54}$$

$$-\tilde{p}_\mathrm{f}^{(0)} + \tilde{\tau}_{zz}^{(0)} - \Sigma k^2\tilde{u}_z^{(0)} = -\tilde{p}_g^{(0)} + \left(\frac{1}{\Gamma} - \mathrm{i}kc^{(0)}\eta_\mathrm{r}^{(0)}\right)2\mathrm{d}_z\tilde{u}_z^{(0)}. \tag{55}$$

Comparing the above tangential velocity condition, Eq. (53), with the original tangential velocity condition (Eq. 23), it can be seen that the second term in the left side of Eq. (23) is absent in the above simplified equation. The term $\tilde{u}_z$ in the left side of the original Eq. (23) represents a coupling between the base flow and interfacial fluctuations due to the discontinuity of the base flow velocity gradient at the interface, and this term was shown to be responsible for the low-*Re* instability of Newtonian plane Couette flow by Kumaran et al. [3], and by Shankar and Kumar [10] for viscoelastic plane Couette flow in the creeping flow limit. In the present low-*Re* asymptotic analysis, however, that particular term does not appear at leading order in the tangential velocity condition.

The leading order governing equations (35) and (51) can be analytically solved to give the following solutions for $\tilde{v}_z^{(0)}$ and $\tilde{u}_z^{(0)}$:

$$\begin{aligned}\tilde{v}_z^{(0)} = {} & A_1\,\exp[kz] + A_2\,\exp[-kz] \\ & + A_3\,\exp[k(-\mathrm{i}W + \sqrt{1 + W^2 - (c^{(0)})^2 W})z] \\ & + A_4\,\exp[-k(\mathrm{i}W + \sqrt{1 + W^2 - (c^{(0)})^2 W})z],\end{aligned} \tag{56}$$

$$\begin{aligned}\tilde{u}_z^{(0)} = {} & B_1\,\exp[kz] + B_2\,\exp[-kz] + B_3\,\exp[\gamma z] \\ & + B_4\,\exp[-\gamma z],\end{aligned} \tag{57}$$

where $\gamma = k\sqrt{1 - \Gamma(c^{(0)})^2/(1 - \mathrm{i}kc^{(0)}\eta_\mathrm{r}^{(0)}\Gamma)}$, and the constants $\{A_1 \cdots A_4\}$ and $\{B_1 \cdots B_4\}$ must be determined from the boundary and interface conditions. The above leading order solutions are substituted in the interface conditions, Eqs. (52)–(55), as well as in the four boundary conditions at $z = 1$ and $z = -H$, and this system of equations is expressed in matrix form as $\mathbf{Ax} = 0$, where $\mathbf{A}$ is an 8×8 matrix containing the eight conditions, and $\mathbf{x}$ is the vector of eight constants $\{A_1 \cdots B_4\}$. The determinant of the matrix $\mathbf{A}$ is set to zero to obtain the characteristic equation.

The leading order wavespeed $c^{(0)}$ is a function of Γ, W, k, H, $\eta_\mathrm{r}^{(0)}$ and Σ. When $\Gamma \to 0$, the fluid viscous stresses are very small compared to the solid elastic stresses, and so one recovers the rigid wall limit. In this limit, we expect to obtain the HFGL solutions for $c^{(0)}$ in a rigid channel outlined in the previous section. In this section, we want to explore the effect of increasing the solid layer deformability, i.e. increasing Γ from zero, on the HFGL modes. To this end, for fixed values of W, k, H, $\eta_\mathrm{r}^{(0)}$, Σ, we specify a numerical value of Γ and calculate $c^{(0)}$ using the symbolic package *Mathematica*. Results from our calculations show that while the leading order solutions are purely real for HFGL modes in a rigid channel, *the leading order solutions for $c^{(0)}$ are complex when the wall is deformable*. For small values of Γ, the imaginary part of $c^{(0)}$ is *positive* (system unstable) for downstream traveling waves (real part of $c^{(0)}$ is positive), and the imaginary part of $c^{(0)}$ is *negative* for upstream traveling waves (real part of $c^{(0)}$ negative). Interestingly, the imaginary part of $c^{(0)}$ for downstream and upstream traveling waves has the same magnitude, but opposite signs; simply put, if the complex number $c^{(0)}$ is written as $a + \mathrm{i}b$ (a, b positive) for downstream waves, then the result for upstream waves is given by $-a - \mathrm{i}b$. Figs. 4 and 5 show the variation of $c_\mathrm{i}^{(0)}$ with Γ for the first two HFGL modes, and this shows that the HFGL modes become unstable as the solid wall becomes deformable. As Γ is increased, $c_\mathrm{i}^{(0)}$ oscillates between stable and unstable regions. Also, the two curves in $c_\mathrm{i}^{(0)}$ versus Γ plots for upstream and downstream traveling waves differ only in sign, and have the same magnitude for all values of Γ. In other words, when the downstream traveling waves are unstable (stable), the upstream traveling waves are stable (unstable). For downstream traveling waves, Fig. 6 shows that $c_\mathrm{i}^{(0)} \propto \Gamma^2$ for $\Gamma \ll 1$, i.e. in the limit very small solid deformability. Furthermore, wall deformability is found to have a destabilizing effect on all the discrete HFGL modes.

It is instructive to contrast this result with the previous instability of UCM plane Couette flow past a deformable wall analyzed by Shankar and Kumar [10]. In their analysis, fluid and solid inertia were neglected in the creeping flow limit, and the instability was primarily driven by the coupling between the base flow and interfacial fluctuations through the tangential continuity condition (Eq. (23)). However, in the present asymptotic analysis, the coupling term *does not* appear in the tangential velocity condition at leading order (see Eq. (53)). In contrast, in the present case, the coupling between base flow and fluctuations occurs in the governing equations due to the nonlinear upper-convected terms in the UCM constitutive relation, and via the stress continuity conditions at the interface. Furthermore, the inertial terms in the fluid and the solid medium appear in the leading order problem despite the $Re \ll 1$ limit, in marked contrast with the earlier analysis of Shankar and Kumar [10]. Another important difference is that in the earlier analysis of [10], the flow becomes unstable only if Γ is greater than a certain critical value in the $Re = 0$ limit, and this critical value is

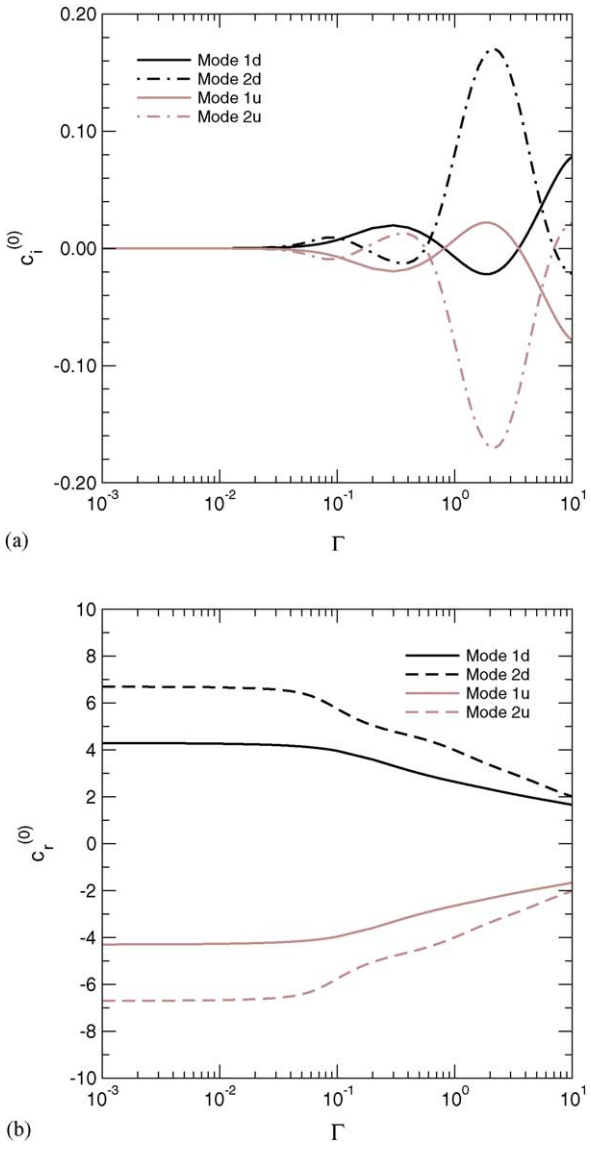

Fig. 4. Effect of wall deformability on HFGL modes. Asymptotic results for $W = 2$, $k = 1$, $\eta_r^{(0)} = 0$, $H = 1$, $Re \to 0$. Results for upstream and downstream waves are denoted by the letters 'u'and 'd' after the mode numbers. (a) $c_i^{(0)}$ vs. Γ; (b) $c_r^{(0)}$ vs. Γ.

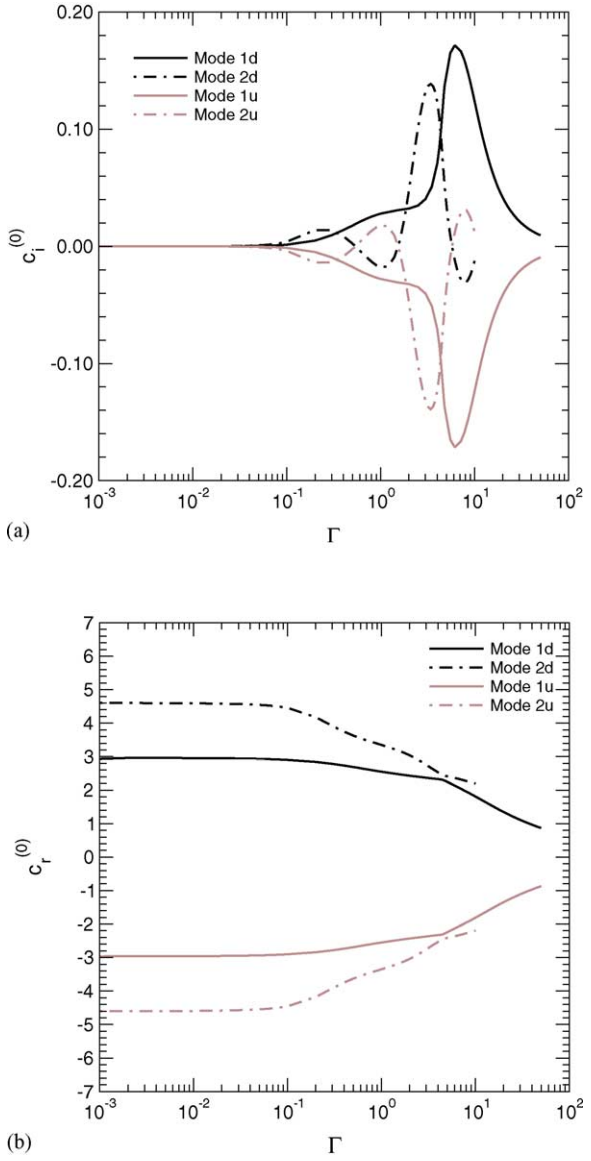

Fig. 5. Effect of wall deformability on HFGL modes. Asymptotic results for $W = 5$, $k = 1$, $\eta_r^{(0)} = 0$, $H = 1$, $Re \to 0$. Results for upstream and downstream waves are denoted by the letters 'u'and 'd' after the mode numbers. (a) $c_i^{(0)}$ vs. Γ; (b) $c_r^{(0)}$ vs. Γ.

an O(1) quantity. Whereas, in the instability of the HFGL modes due to wall deformability, for small values of Γ, $c_i^{(0)} \propto \Gamma^2$ and is positive for downstream waves, and so even a small Γ is sufficient for the present instability.

In the above discussion, we have considered only the leading order wavespeed $c^{(0)}$, which becomes unstable when Γ is increased from zero. Here, we show that for downstream traveling waves, it is possible to account for the first correction to the wavespeed from the earlier analysis of GL [11] in the limit of small wall deformability $\Gamma \ll 1$. First, our asymptotic results for $Re \ll 1$ and $\Gamma \ll 1$ can be written for *downstream* traveling waves, after noting that $c_i^{(0)} \propto \Gamma^2$ in this limit, as:

$$c = Re^{-1/2}\, c^{(0)} = Re^{-1/2}[c_r^{(0)} + c_i^{(0)}] = Re^{-1/2}[c_r^{(0)} + \mathrm{i}a\Gamma^2], \tag{58}$$

where a is a positive real constant which is due to the small wall deformability, and for $\Gamma \ll 1$ (the limit of very small wall deformability), $c_r^{(0)}$ in the above equation is the same as that found for rigid channels. In the earlier analysis of GL [11], they also calculated the first correction to the wavespeed $c^{(1)}$ for the rigid channel problem as

$$c = Re^{-1/2}\, c^{(0)} + c^{(1)}. \tag{59}$$

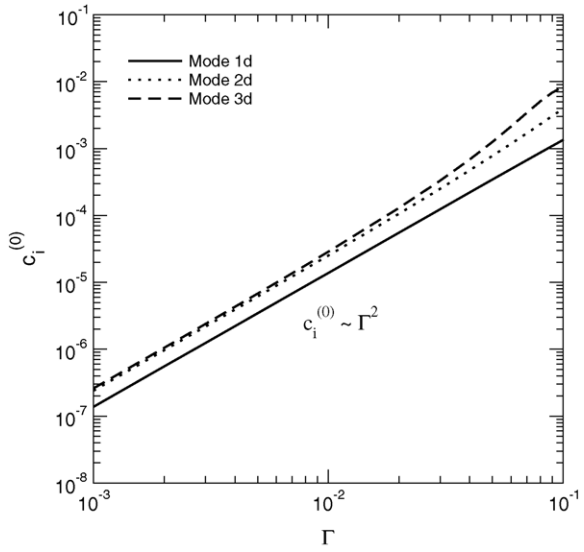

Fig. 6. Scaling of $c_i^{(0)}$ with Γ for small Γ from asymptotic analysis. Data showing $c_i^{(0)} \sim \Gamma^2$ scaling for $W = 5$, $k = 1$, $\eta_r^{(0)} = 0$, $H = 1$, $Re \to 0$ for the case of downstream waves.

GL demonstrate that the imaginary part of $c^{(1)}$ is negative for rigid channels, and the above equation can therefore be written as

$$c = Re^{-1/2}\, c_r^{(0)} + d - \mathrm{i}b, \tag{60}$$

where $-b$ is the imaginary part of the first correction ($b > 0$), $c_r^{(0)}$ in Eqs. (60) and (58) are the same quantities, and d is the real part of the first correction whose sign is irrelevant to the present discussion. Assuming that the above first correction will be unchanged in the limit of small Γ for the case of UCM flow past a deformable wall, it is possible to combine our leading order asymptotic result with the first correction result of GL to give:

$$c = Re^{-1/2}[c_r^{(0)} + \mathrm{i}a\Gamma^2 - \mathrm{i}b\, Re^{1/2} + d\, Re^{1/2}]. \tag{61}$$

This is the expected result for c including the effect of small wall deformability ($\Gamma \ll 1$) on the HFGL modes. Considering only the imaginary part of c in the above equation, it can be seen that for neutral stability in the limit of $Re \ll 1$ and $\Gamma \ll 1$, we require $a\Gamma^2 = b\, Re^{1/2}$, or $\Gamma \propto Re^{1/4}$ for neutral modes in the case of downstream waves.

Thus, the important conclusions from our $Re \ll 1$ asymptotic analysis of the HFGL modes can be summarized as follows: (1) all the HFGL modes become unstable when the deformability of the wall is increased. (2) As Γ is in-

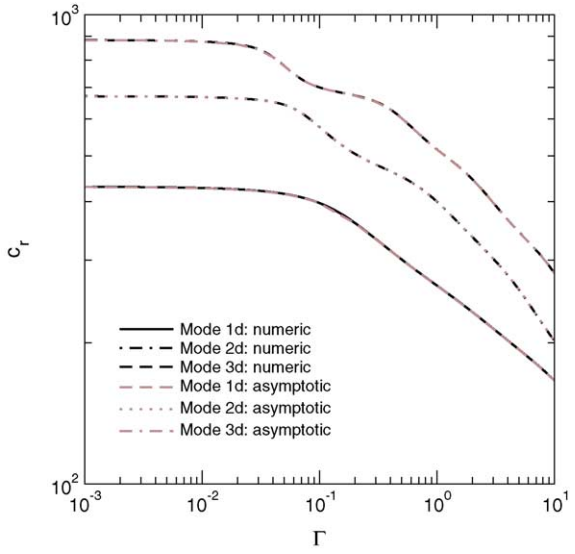

Fig. 7. Effect of wall deformability (Γ) on c_r: comparison of numerical and asymptotic results for $W = 2$, $H = 1$, $k = 1$, $Re = 10^{-4}$, $\eta_r = 0$, $\Sigma = 0$. Data shown for downstream waves.

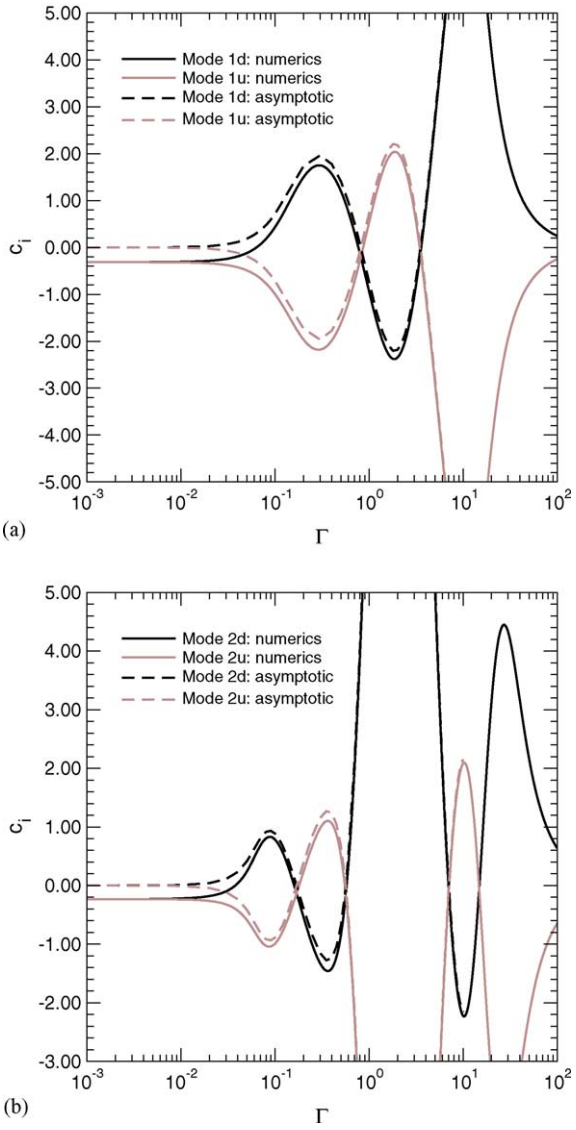

Fig. 8. Effect of wall deformability (Γ) on c_i: Comparison of numerical and asymptotic results for results for $W = 2$, $k = 1$, $H = 1$, $Re = 10^{-4}$, $\eta_r = 0$, $\Sigma = 0$. (a) Mode 1; (b) Mode 2.

creased, the $c_i^{(0)}$ versus Γ curves show oscillations between stable and unstable regions, with the variation for downstream traveling waves being completely antiphase with that for upstream traveling waves. Thus, when downstream traveling waves are unstable (stable), upstream traveling waves are stable (unstable). (3) The imaginary part of the leading order wavespeed for downstream waves is positive even for very small values of Γ, and $c_i^{(0)} \propto \Gamma^2$ in this limit. (4) In the limit of small Re, the viscosity ratio η_r in the solid layer should be $O(Re^{1/2})$ for this instability to exist. (5) In the limit of small Re and Γ, it is argued (after *qualitatively* taking the first correction into account) that $\Gamma \propto Re^{1/4}$ for neutrally stable modes in the case of downstream waves.

4.1.1. Extension to Oldroyd-B fluid

It is useful here to examine the applicability of the above asymptotic results to the Oldroyd-B fluid with nonzero solvent viscosity ratio β. To this end, we substitute the scalings introduced in the foregoing discussion (Eqs. (34)–(40)) in the linearized momentum equations for the Oldroyd-B fluid (Eqs. (29) and (30)). It can be readily verified that in order for the solvent viscous stresses in the momentum equations to be of the same order as the polymer stresses and the inertial stresses in the Oldroyd-B fluid, it is necessary to stipulate that $\beta \sim Re^{1/2} \ll 1$, implying the limit of zero solvent viscosity ratio at very low Re. For finite β, the solvent viscous stresses are $O(Re^{-1/2})$ larger than the inertial stresses and the polymer stresses in the fluid; therefore, the polymer stresses and

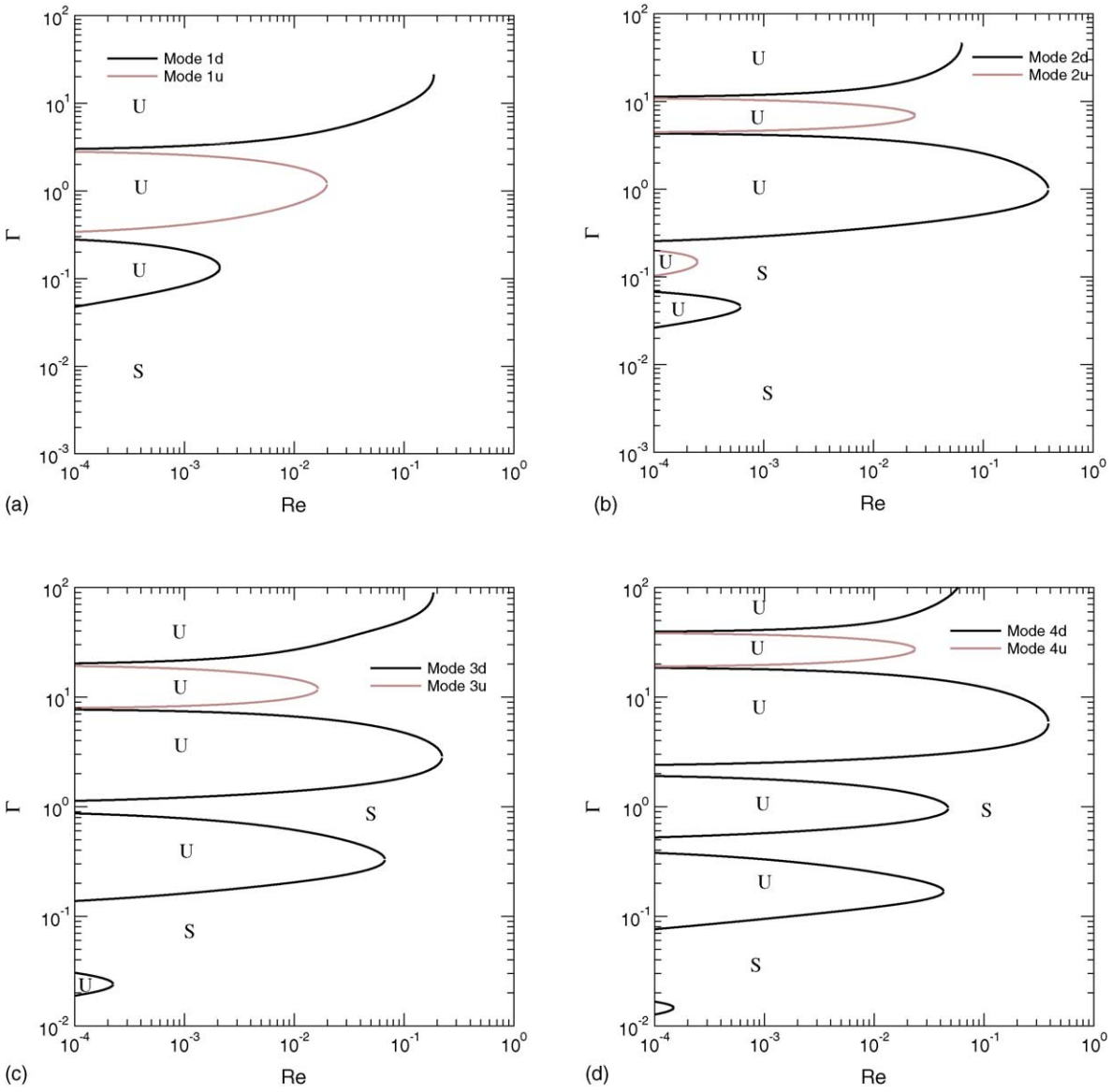

Fig. 9. Neutral stability curves in the Γ–Re plane, for $W = 1$, $H = 1$, $k = 1$, $\eta_r = 0$, $\Sigma = 0$. 'S' and 'U' denote stable and unstable regions, and neutral curves for upstream and downstream waves are shown in gray and black curves respectively. (a) Mode 1; (b) Mode 2; (c) Mode 3; (d) Mode 4.

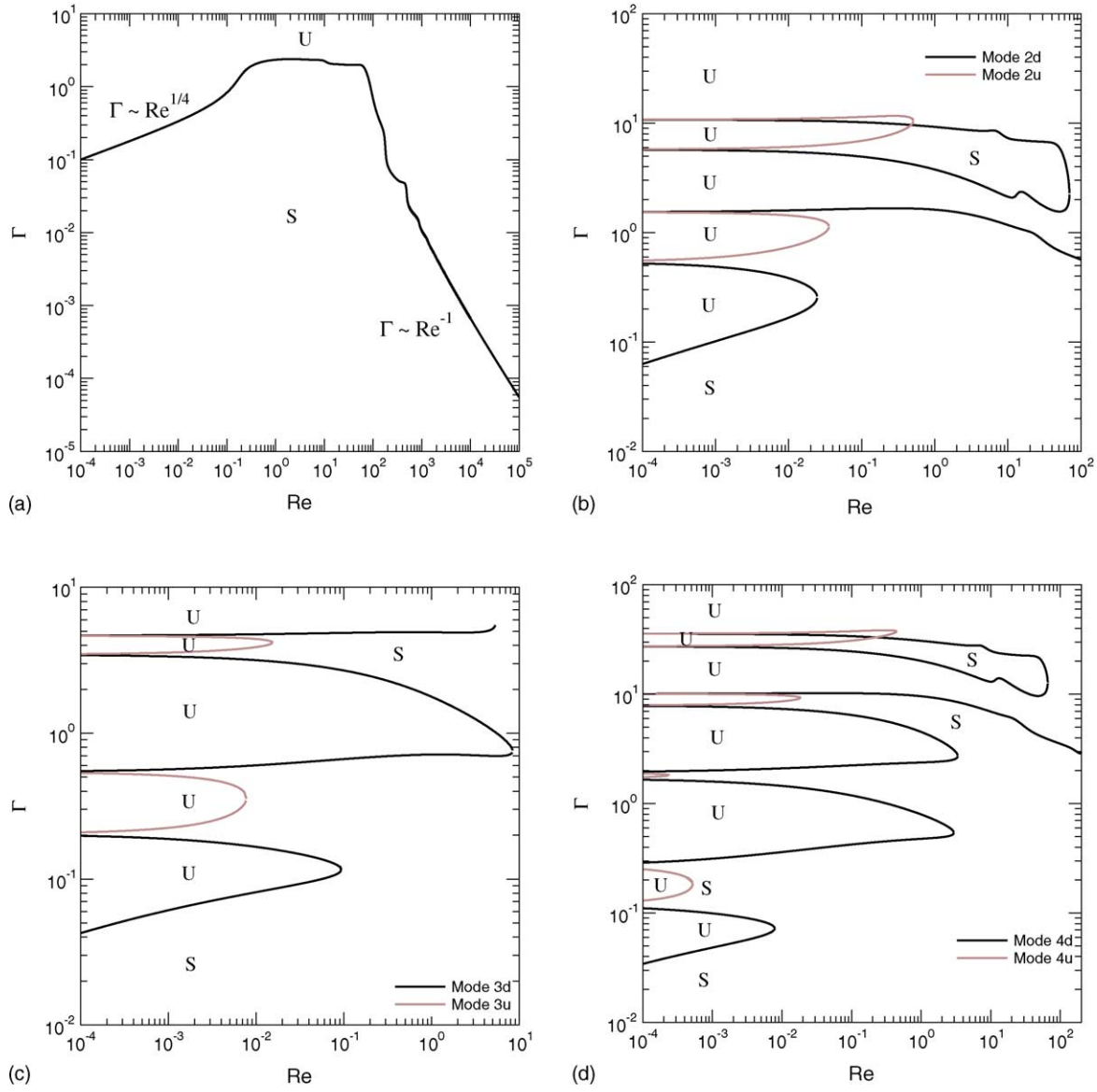

Fig. 10. Neutral stability curves in the Γ–Re plane, for $W = 5$, $H = 1$, $k = 1$, $\eta_r = 0$, $\Sigma = 0$. 'S' and 'U' denote stable and unstable regions, and neutral curves for upstream and downstream waves are shown in gray and black curves respectively. (a) Mode 1; (b) Mode 2; (c) Mode 3; (d) Mode 4.

the inertial stresses do not appear at leading order, and one recovers a Newtonian fluid. Because a Newtonian fluid does not admit elastic shear waves, there are no solutions to c at this order. Consequently, the instability of the HFGL modes is not present for Oldroyd-B fluid at very low Re for finite values of solvent viscosity ratio. This discussion thus suggests that the presence of solvent viscosity has a stabilizing effect on the HFGL instability. However, at finite $Re \sim O(1)$, it is not possible to neglect the polymer stresses and inertial stresses in the Oldroyd-B fluid, and it is possible that the HFGL mode instability of the UCM fluid continues to be present in the Oldroyd-B fluid with nonzero solvent viscosity ratio for finite Re. This indeed turns out to be the case, as we demonstrate numerically in Section 4.2.2.

4.2. Results from numerical method

In this section, we examine the effect of wall deformability on the HFGL modes at finite Re using the numerical method described in Section 2.4. We use the asymptotic results from the previous section as starting guesses for the numerical method. The asymptotic analysis of the previous section gives rise to the following issues and questions which will be addressed using the numerical method: (1) The asymptotic results are valid in the limit $Re \ll 1$; will this instability persist at intermediate and high Re? (2) How does the finite-Re continuation of the HFGL mode instability due to wall deformability contrast with the finite-Re continuation of the instability analyzed by Shankar and Kumar [10],

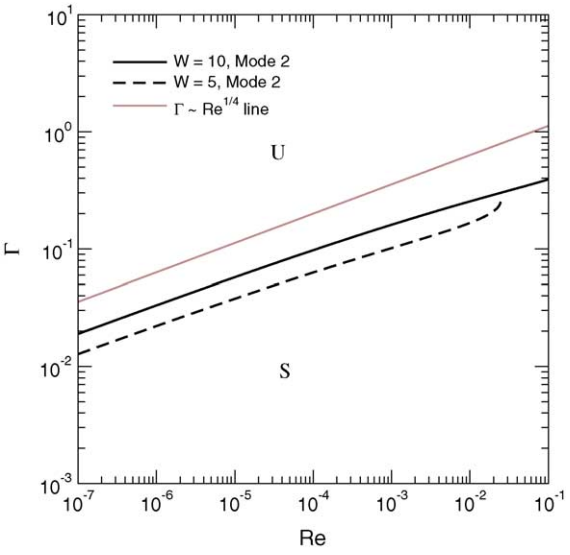

Fig. 11. Scaling of Γ with Re for small Re: numerical data showing $\Gamma \sim Re^{1/4}$ scaling for $k = 1$, $\eta_r^{(0)} = 0$, $H = 1$, $\Sigma = 0$, in agreement with asymptotic prediction for downstream waves.

who showed that the ZRGL mode becomes unstable in the creeping flow limit when the wall is made sufficiently deformable? (3) The low-Re asymptotic analysis in the previous section requires that the solid–fluid viscosity ratio η_r should scale as $Re^{1/2}$ in the $Re \ll 1$ limit in order for the instability to exist. What is the effect of increasing Re on this restriction on η_r ? Will the instability be present for finite values of η_r at finite Re? (4) The previous analysis of Shankar and Kumar [10] also showed that the instability of the ZRGL mode due to wall deformability is essentially a continuation of the instability already present in Newtonian fluids [3], modified by the fluid viscoelastic effects. Will the present instability of the HFGL modes due to wall deformability be present in the limit of Newtonian fluids, i.e., for $W \ll 1$?

To answer the above questions, we now turn to the results from our numerical method. Figs. 7 and 8 show the comparison of the results obtained from the asymptotic analysis described in the previous section with the numerical results obtained by solving the complete linear stability equations. In the plot of c_i versus Γ in Fig. 8, it is clear that for downstream waves, the asymptotic result for c_i is positive in the limit of $\Gamma \to 0$, while the numerical (and exact) result for c_i is negative up to a critical value of Γ. The asymptotic prediction is always positive in the limit of small Γ because we have not calculated the first correction to the wavespeed (which has

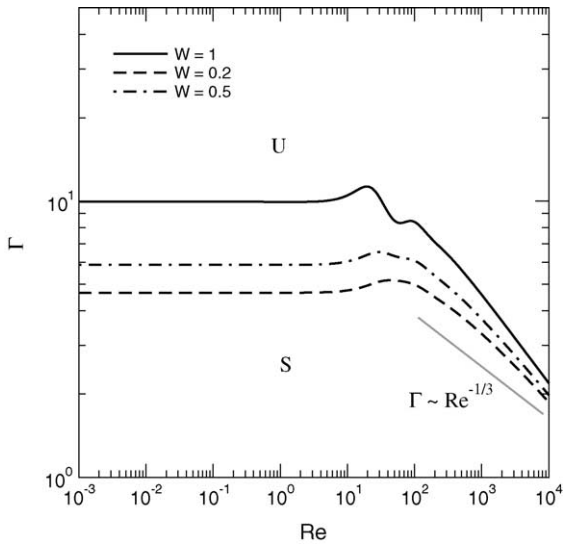

Fig. 12. Neutral stability curve in the Γ–Re plane for the ZRGL mode destabilized by wall deformability: continuation of the zero-Re results of Shankar and Kumar [10] to finite and large Re.

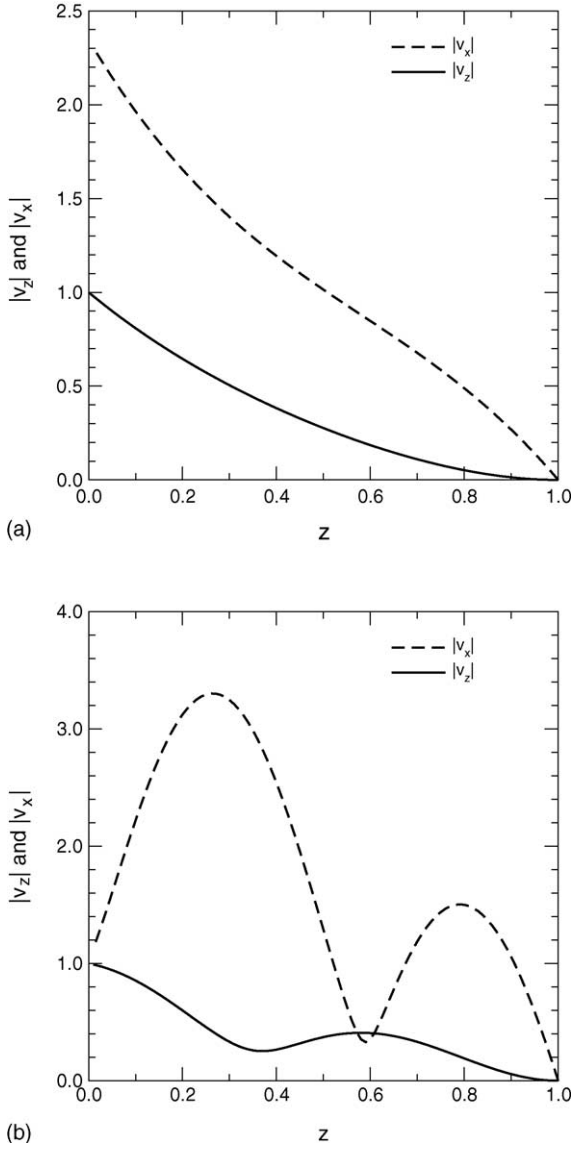

Fig. 13. Fluid velocity eigenfunction plots for ZRGL and HFGL modes past a deformable wall: data for $W = 1$, $H = 1$, $k = 1$. (a) $Re = 10^{-4}$, $\Gamma = 9.93$, $c_r = 0.253$, $c_i = 0$; ZRGL mode. (b) $Re = 1$, $\Gamma = 1$, $c_r = 6.64$, $c_i = -0.54$; HFGL mode.

a stabilizing effect) in the present analysis. This observation is also consistent with the prediction in Section 4.1 that at a given nonzero *Re*, there exists a critical value of $\Gamma \propto Re^{1/4}$ for downstream waves to be unstable. In the plots shown in Fig. 8, $Re = 10^{-4}$, and so it takes a finite (but numerically small) value of Γ for the downstream waves to be unstable. However, the asymptotic and numerical results agree very well when $\Gamma \sim O(1)$ for both downstream and upstream waves, because the stabilizing effect of the first correction diminishes since it is $O(Re^{1/2})$ smaller than the leading order wavespeed. The agreement between asymptotic and numerical results for c_r as a function of Γ in Fig. 7 is also very good.

In order to determine whether the predicted instability persists at finite *Re*, neutral stability curves were computed in the Γ–*Re* plane, for the first few HFGL modes and for a given set of parameters W, k, η_r, Σ, H. These neutral curves are shown in Figs. 9–10. Let us first focus on Fig. 9. We use the letter 'u' after the mode number to indicate upstream waves, and the letter 'd' after the mode number for downstream waves in the following discussion and figures. In Fig. 9, the unstable regions for all the modes extend only up to a small (but finite) *Re*. Also, there are alternating regions in the parameter space in which the downstream/upstream modes are stable or unstable. This is essentially a consequence of the oscillatory variation of c_i with Γ shown in Fig. 8. In these figures, $W = 1$, and the maximum *Re* up to which the instability persists is around 0.1. However, when *W* is increased to 5 in Fig. 10, the nature of the neutral curves changes drastically. Fig. 10(a) shows the neutral curve for mode 1d (of the HFGL family) extends up to very high *Re*, and $\Gamma \propto Re^{-1}$ in the limit of large *Re*. However, mode 1u does not become unsta-

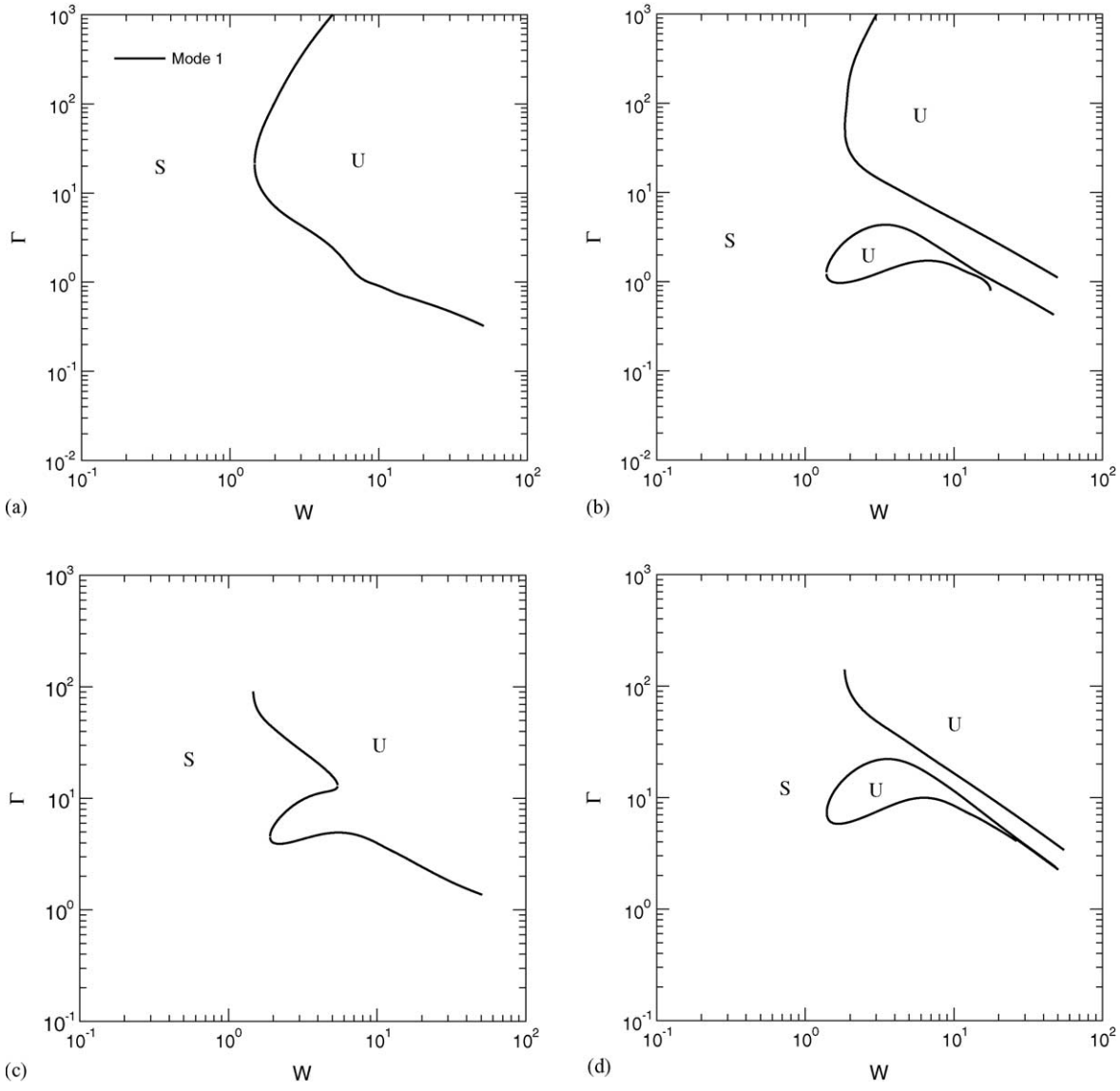

Fig. 14. Neutral stability curves in the Γ–*W* plane, for $Re = 1$, $H = 1$, $k = 1$, $\eta_r = 0$, $\Sigma = 0$. 'S' and 'U' denote stable and unstable regions respectively. Data shown only for downstream waves. (a) Mode 1; (b) Mode 2; (c) Mode 3; (d) Mode 4.

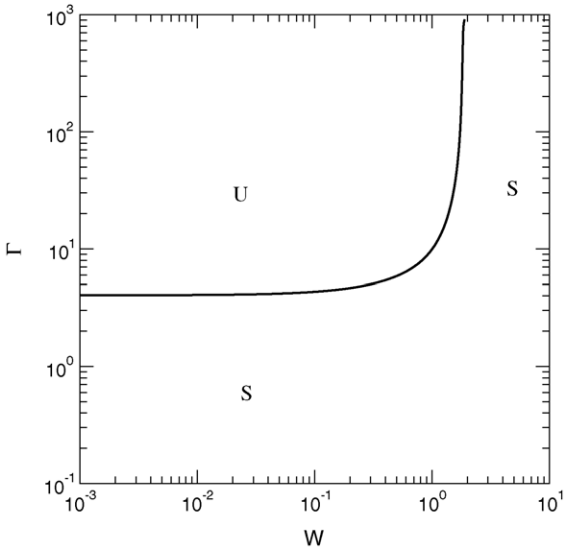

Fig. 15. Neutral stability curve in the Γ–W plane for the ZRGL mode destabilized by wall deformability: Data for $Re = 1$, $H = 1$, $k = 1$, $\eta_r = 0$, $\Sigma = 0$.

ble upon increasing Γ at any Re. This can also be seen in the $c_i^{(0)}$ versus Γ curve from the asymptotic analysis shown in Fig. 5(a). The other curves in Fig. 10 show that while there exist alternating stable and unstable regions, the instability persists up to $Re \sim 10^2$. Data for $W = 10$ (not displayed in this paper), along with the data presented here for $W = 1$ and 5, confirm that the Re up to which the instability persists increases with an increase in W. Fig. 11 shows that for $Re \ll 1$, $\Gamma \sim Re^{1/4}$ for neutrally stable downstream waves, in agreement with the prediction of the asymptotic analysis of Section 4.1.

Fig. 12 shows the neutral curve in the Γ–Re plane for the continuation of the instability predicted in the creeping flow limit by Shankar and Kumar [10]. In that study, the authors showed that the ZRGL mode becomes unstable in the $Re = 0$ limit upon increasing wall deformability, and also that this unstable mode is essentially a continuation of the already existent Newtonian fluid instability [3] to finite W. We continued the $Re = 0$ result of that paper to finite Re, and the neutral curves in Fig. 12 for different values of W show that the instability continues to high Re, and that $\Gamma \sim Re^{-1/3}$ in the limit of high Re. This scaling is similar to that reported for Newtonian plane Couette flow past a deformable wall at high Re by Srivatsan and Kumaran [20]. However, these neutral curves are qualitatively different from the neutral curves discussed for the HFGL family of modes. In particular the high Re scaling $\Gamma \sim Re^{-1}$ shown in Fig. 10(a) for the continuation of the HFGL mode is very different from the $\Gamma \sim Re^{-1/3}$ scaling obtained for the continuation of the ZRGL mode. This demonstrates that the two instabilities are driven by qualitatively different mechanisms. Comparing the data for $W = 1$ shown for the two different instabilities in Figs. 9 and 12, it is clear that the Γ values required for destabilizing the HFGL family of modes are typically very small compared to that required for the ZRGL mode, when the HFGL instability exists. For $W = 5$, the ZRGL mode is always stable for the chosen value of $H = 1$, and so this instability is absent. However, the continuation of HFGL modes do become unstable for $W = 5$, as shown in Fig. 10. Thus, these data show that, at finite W, the instability due to the continuation of the HFGL modes is a powerful mechanism compared to the continuation of the ZRGL mode. It is instructive to consider the variation of the amplitude of perturbation velocities $|\tilde{v}_z|$ and $|\tilde{v}_x|$ with z, which further demonstrate the difference between the ZRGL and HFGL modes. This is displayed in Fig. 13. While calculating these eigenfunctions, we fix the amplitude of the normal velocity component $|\tilde{v}_z| = 1$ at the fluid–solid interface $z = 0$. Fig. 13(a) shows the variation for the ZRGL mode, while Fig. 13(b) shows the variation for the HFGL mode, and $W = 1$ in both the cases. For the ZRGL mode, the variation is monotonic from $z = 0$ to $z = 1$, but the HFGL mode eigenfunctions exhibit oscillatory variation. Oscillatory variation of the eigenfunctions is a signature of the importance of elastic effects in HFGL modes, while the absence of this in the ZRGL modes indicates that fluid elasticity does not play an important role in the ZRGL instability. This further suggests that the HFGL modes are absent in Newtonian fluids, and that the ZRGL mode instability is similar to the instability of a Newtonian fluid flowing past a deformable wall.

Figs. 14 and 15 show the neutral stability curves in the Γ–W plane for both HFGL modes and the ZRGL mode. The data for the ZRGL mode (Fig. 15) clearly shows that the instability in the UCM fluid is a continuation to finite W of the already existent Newtonian fluid instability. Also, the instability exists only in a finite region of the Γ–W plane, and is absent when W increases beyond a critical value (around 1 for the data shown in this figure). In marked contrast, the results for the HFGL mode (Fig. 14) show that the unstable region exists for finite and large W, and is absent when $W \to 0$. We show the data only for downstream modes, and the data for upstream modes are qualitatively similar. This comparison shows that the *HFGL mode instability past a deformable wall predicted in this study is fundamentally due to the viscoelastic nature of the fluid, and is absent in Newtonian fluids*. This is one of the central results of this paper.

Fig. 16 show the neutral stability curves in the Γ–k plane for both HFGL and ZRGL modes past a deformable wall. For the case of HFGL modes (Fig. 16(a)–(c)), these results show that the instability is absent in the limit of low wavenumbers, but exists for finite and large k. In contrast, Fig. 16(d) displays the neutral curve for the continuation of the ZRGL mode which shows that only a finite band of wavenumbers become unstable for this case. Fig. 17 examines the effect of the interfacial tension between the fluid and the deformable solid, in order to ascertain whether the large-k modes are stabilized by nonzero interfacial tension. For the case of the instability of ZRGL modes due to the deformable wall, nonzero interfacial tension has a stabilizing effect on large-k unstable modes.

However, the results in Fig. 17 shows that the interfacial tension does not stabilize the continuation of HFGL modes. This suggests that the destabilization of the HFGL modes by wall deformability is not an 'interfacial instability', and this result is also in marked contrast with the continuation of the ZRGL modes. It should be noted here that the UCM model used here to describe the viscoelastic fluid does not have any solvent contribution to the fluid stress, and the use of an Oldroyd-B model has a stabilizing effect on these high-k unstable modes.

It is appropriate here to remark on the validity of the linear viscoelastic model used here to describe the deformation in the solid. The base state x–directional strain in the solid wall (Eq. (9)) is proportional to the nondimensional quantity Γ, and so strictly speaking the linear elastic solid model is valid only for $\Gamma \ll 1$. The study by Gkanis and Kumar [19] for the case of Newtonian plane Couette flow past a neo-Hookean solid (accounting for finite strains) showed however that for wall thickness $H > 2$, the agreement between the linear and nonlinear solid models was very good even for $\Gamma \sim \mathrm{O}(1)$. For the present class of modes, however, $\Gamma \sim 0.1$ (or even smaller) for destabilization by the deformable solid wall, and so the present predictions are expected to be accurate despite the use of a simple linear viscoelastic model for the solid. The data presented for larger values of Γ, however, may be modified somewhat upon using a more complex model for the solid deformation.

4.2.1. Results for nonzero solid viscosity ratio η_r

The asymptotic analysis of Section 4.1 required that $\eta_r \sim \mathrm{O}(Re^{1/2})$ in the limit $Re \ll 1$ in order for the elastic stresses in the solid to be as large as the viscous stresses in the solid.

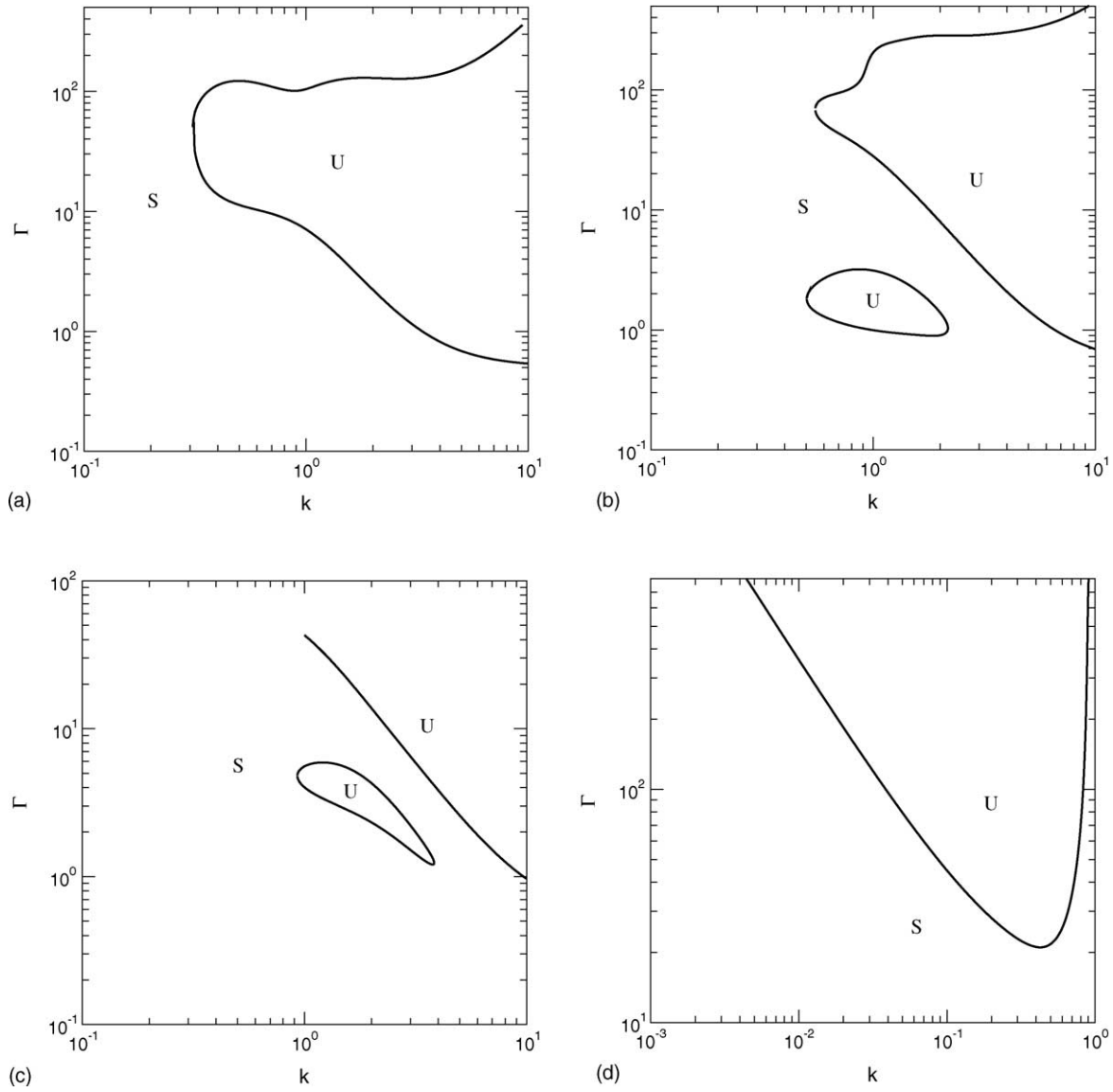

Fig. 16. Neutral stability curves in the Γ–k plane, for $Re = 1$, $W = 2$, $H = 1$, $\eta_r = 0$, $\Sigma = 0$. 'S' and 'U' denote stable and unstable regions respectively. Data shown only for downstream waves for HFGL modes 1–3. (a) Mode 1; (b) Mode 2; (c) Mode 3; (d) ZRGL mode.

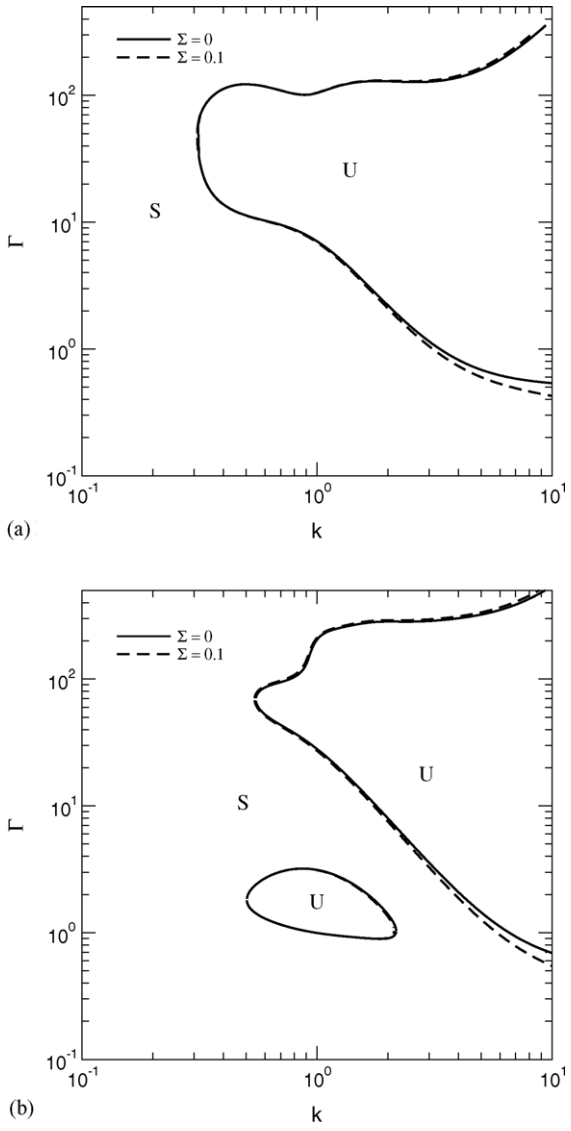

Fig. 17. Neutral stability curves in the Γ–k plane, for $Re = 1$, $W = 2$, $H = 1$, $\eta_r = 0$. Effect of nonzero interfacial tension Σ between the fluid and the solid. 'S' and 'U' denote stable and unstable regions respectively. Data shown only for downstream waves. (a) Mode 1; (b) Mode 2.

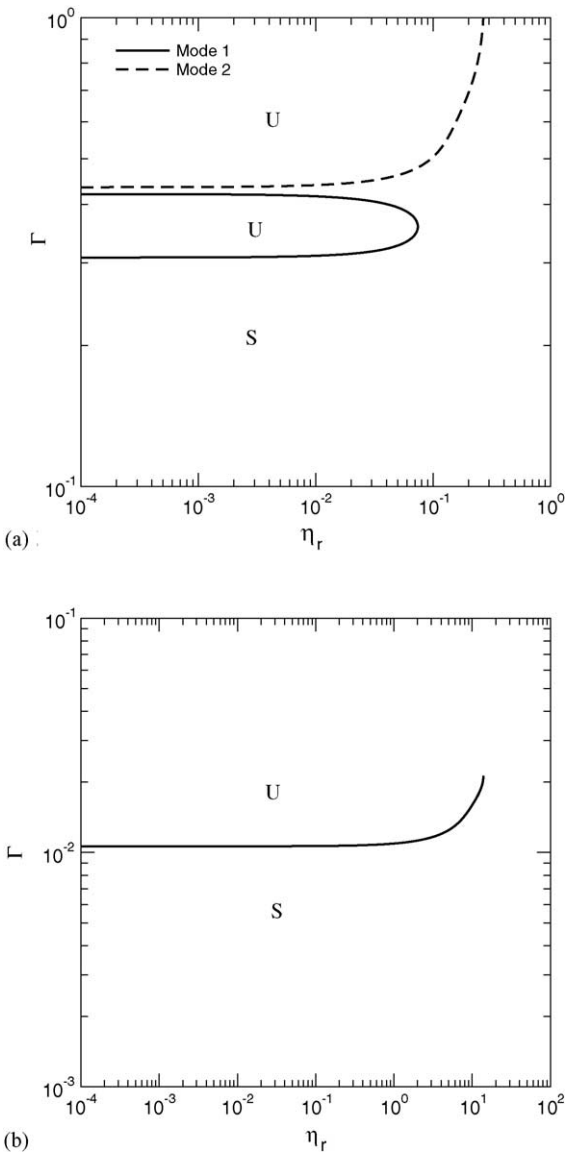

Fig. 18. Neutral stability curves in the Γ–η_r plane, for $H = 1, k = 1$, $\Sigma = 0$. Effect of nonzero viscosity ratio, η_r, between the solid and the fluid. 'S' and 'U' denote stable and unstable regions respectively. Data shown only for downstream waves. (a) $W = 15$, $Re = 150$; (b) $W = 5$, $Re = 1000$.

However, when Re becomes finite, one may expect this restriction on the smallness of η_r to relax. To this end, we examined the effect of η_r on the predicted instability at finite values Re, and this variation is shown in Fig. 18. These figures show that as Re increases the range of η_r up to which the instability persists also increases, and the instability exists for $\eta_r \sim O(1)$ values.

4.2.2. Results for Oldroyd-B fluid

In this section, we present preliminary numerical results for the stability of plane Couette flow of an Oldroyd-B fluid past a deformable wall. The arguments presented in Section 4.1.1 indicate that the HFGL mode instability will not be present in an Oldroyd-B fluid in the limit of low Re for finite values of solvent viscosity ratio β. However, it is likely that the results presented in the preceding section for the UCM fluid ($\beta = 0$) at finite Re must extend to the case of nonzero values of β. Fig. 19 shows the variation of Γ required for destabilizing the flow with β, for two different values of W and Re. These results show that the HFGL instability of the UCM fluid flow past a deformable wall indeed continues to nonzero values of β, and that the solvent viscosity has a stabilizing effect on the HFGL instability. The instability ceases to exist beyond $\beta \simeq 0.18$, and this suggests that the instability could be potentially realized only in concentrated polymer solutions. Fig. 20 shows the variation of Γ with Re for a fixed value of $\beta = 0.15$. This demonstrates that the instability is

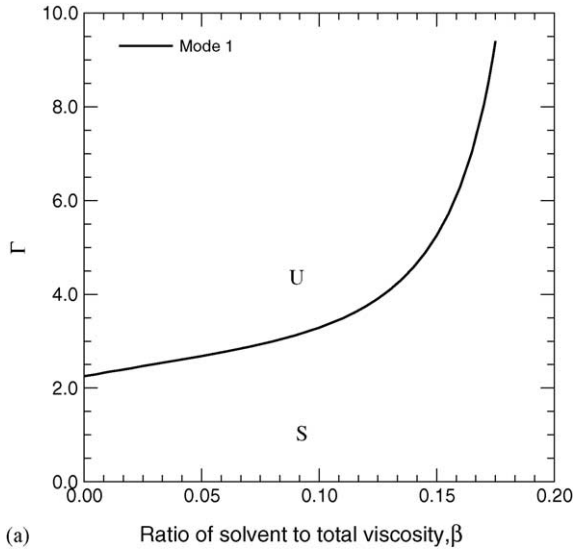

Fig. 19. Neutral stability curves in the Γ–β plane, for $H = 1, k = 1, \Sigma = 0$. Effect of nonzero solvent viscosity ratio, β, in an Oldroyd-B fluid on the predicted instability. 'S' and 'U' denote stable and unstable regions respectively. Data shown only for downstream waves. (a) $W = 5$, $Re = 10$; (b) $W = 15$, $Re = 1000$.

present only at finite *Re* and is absent for low *Re*, in agreement with the discussion in Section 4.1.1.

5. Summary and conclusions

The effect of wall deformability on high-frequency, low-*Re* GL (HFGL) modes in the plane Couette flow of an UCM fluid was analyzed using both asymptotic analysis (at low *Re*) and numerical solutions (at arbitrary *Re*). We first showed that for the case of rigid-walled channels, the numerically computed discrete spectrum of eigenvalues (using spectral

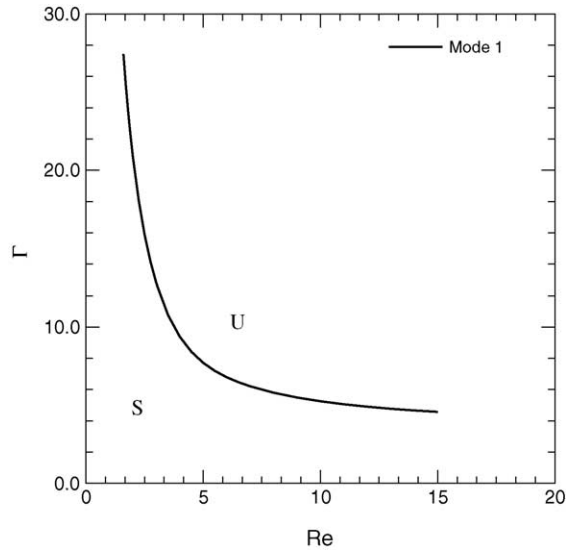

Fig. 20. Neutral stability curve in the Γ–*Re* plane for the HFGL mode in an Oldroyd-B fluid for nonzero solvent viscosity ratio $\beta = 0.15$: Data for $W = 5, k = 1, H = 1, \Sigma = 0$. 'S' and 'U' denote stable and unstable regions respectively.

methods) at finite *Re* are nothing but a continuation of the zero Reynolds number (ZRGL) modes and HFGL modes analyzed by GL [11]. Thus, the two ZRGL and the many discrete HFGL modes together describe the full discrete spectrum of eigenvalues for UCM plane Couette flow in a rigid channel in the limit of low *Re*, which can be numerically continued to any desired finite *Re*. Our asymptotic analysis on the effect of wall deformability in the limit of low *Re* showed that the all the HFGL family of modes for UCM plane Couette flow become unstable in the low *Re* limit when Γ is increased beyond a certain critical value which is proportional to $Re^{1/4}$ for downstream traveling waves. Upstream traveling waves are stable in the $\Gamma \ll 1$ limit. Interestingly, the variation of the imaginary part of wavespeed (which is proportional to the growth rate) with Γ showed oscillatory variation of the growth rate alternating between stable and unstable regions, for $\Gamma \sim \mathrm{O}(1)$, with the curves for downstream and upstream waves being completely antiphase with each other. Importantly, in our asymptotic analysis the coupling between the base flow and fluctuations did not occur in the tangential velocity condition at the fluid–solid interface, but rather in the governing equations via the upper convected terms of the constitutive relation, and via the stress continuity conditions at the interface between the fluid and the deformable solid. This feature of the present instability is qualitatively different from that analyzed in Kumaran et al. [3] for Newtonian fluids and in Shankar and Kumar [10] for ZRGL modes in UCM plane Couette flow. The asymptotic analysis further requires the solid-fluid viscosity ratio η_r to be $\mathrm{O}(Re^{1/2})$ in the limit of low *Re*, in order for the instability to exist. For an Oldroyd-B fluid, the asymptotic analysis shows that the instability of HFGL modes does not exist in the limit of low *Re* for finite values of solvent viscosity ratio β.

The low-*Re* unstable modes were numerically continued to finite *Re*, and this showed that in most cases the instability persists only up to a finite *Re*, and the *Re* up to which the instability exists increases with an increase in *W*. However, in certain cases, the instability continues to large *Re*, and $\Gamma \propto Re^{-1}$ in the limit $Re \gg 1$. This is in marked contrast with the continuation of the ZRGL mode instability past a deformable wall to high *Re*, which showed that $\Gamma \propto Re^{-1/3}$ for this class of modes. Neutral curves constructed in the Γ–*W* plane showed that while the instability of ZRGL mode due to the deformable wall is essentially the continuation of the Newtonian fluid instability to finite *W*, the HFGL modes exhibit the completely opposite behavior: the HFGL mode instability exists only for finite and large values of *W*, and is absent in the Newtonian fluid limit of $W \to 0$. Although our asymptotic analysis revealed that the HFGL mode instability requires $\eta_r \sim O(Re^{1/2})$ in the limit of low *Re*, numerical computation at finite *Re* showed that the instability persists for $\eta_r \sim O(1)$ values. Neutral stability curves in the Γ–*k* plane further illustrate the difference between the effect of wall deformability on ZRGL modes and HFGL modes. While ZRGL modes are unstable only for a finite band of wavenumbers in the Γ–*k* plane, HFGL modes are unstable for intermediate and large wavenumbers, and they are stable for small wavenumbers. The interfacial tension between the fluid and the deformable solid was shown to have negligible effect on the high-*k* HFGL modes, and this further demonstrates that the present instability is not an 'interfacial instability', rather it occurs due to dynamical processes occurring in the bulk of the viscoelastic fluid which are modified by the deformable solid layer. Preliminary numerical results for the Oldroyd-B model were presented at finite *Re*, and these showed that the HFGL instability of the UCM fluid continues to be present in an Oldroyd-B fluid for solvent viscosity ratio $\beta \simeq 0.2$, and the instability is absent for higher values of β. For a fixed value of β, the instability exists only at finite values of *Re* and is absent in the limit of low *Re*. In conclusion, the present study theoretically predicts a new class of unstable modes in the plane Couette flow of a viscoelastic fluid past a deformable solid wall which arise primarily due to the viscoelastic nature of the fluid, and are *absent* in Newtonian fluids.

References

[1] M.A. Unger, H.-P. Chou, T. Thorsen, A. Scherer, S.R. Quake, Monolithic microfabricated valves and pumps by multilayer soft lithography, Science 288 (2000) 113–116.

[2] A. Groisman, S.R. Quake, A microfluidic rectifier: anisotripic flow resistance at low Reynolds number, Phys. Rev. Lett. 92 (2004) 094501.

[3] V. Kumaran, G.H. Fredrickson, P. Pincus, Flow induced instability of the interface between a fluid and a gel at low Reynolds number, J. Phys. II France 4 (1994) 893–904.

[4] V. Kumaran, Stability of the viscous flow of a fluid through a flexible tube, J. Fluid Mech. 294 (1995) 259–281.

[5] V. Kumaran, Stability of fluid flow through a flexible tube at intermediate Reynolds number, J. Fluid Mech. 357 (1998) 123–140.

[6] V. Kumaran, Stability of wall modes in a flexible tube, J. Fluid Mech. 362 (1998) 1–15.

[7] V. Shankar, V. Kumaran, Stability of non-parabolic flow in a flexible tube, J. Fluid Mech. 395 (1999) 211–236.

[8] V. Shankar, V. Kumaran, Stability of fluid flow in a flexible tube to non-axisymmetric disturbances, J. Fluid Mech. 408 (2000) 291–314.

[9] V. Shankar, V. Kumaran, Stability of wall modes in fluid flow past a flexible surface, Phys. Fluids 14 (2002) 2324–2338.

[10] V. Shankar, S. Kumar, Instability of viscoelastic plane Couette flow past a deformable wall, J. Non-Newtonian Fluid Mech. 116 (2004) 371–393.

[11] V.A. Gorodtsov, A.I. Leonov, On a linear instability of plane parallel Couette flow of viscoelastic fluid, J. Appl. Math. Mech. 31 (1967) 310–319.

[12] H.J. Wilson, M. Renardy, Y. Renardy, Structure of the spectrum in zero Reynolds number shear flow of the UCM and Oldroyd-B liquids, J. Non-Newtonian Fluid Mech. 80 (1999) 251–268.

[13] L. Landau, E. Lifshitz, Theory of Elasticity, Pergamon Press, New York, 1989.

[14] M. Renardy, Y. Renardy, Linear stability of plane Couette flow of an upper convected Maxwell fluid, J. Non-Newtonian Fluid Mech. 22 (1986) 23–33.

[15] M. Renardy, A rigorous stability proof for plane Couette flow of an upper convected Maxwell fluid at zero Reynolds number, Eur. J. Mech. B: Fluids 11 (1992) 511–516.

[16] R. Sureshkumar, A.N. Beris, Linear stability analysis of viscoelastic Poiseuille flow using an Arnoldi based orthogonalization algorithm, J. Non-Newtonian Fluid Mech. 56 (1995) 151–182.

[17] T.C. Ho, M.M. Denn, Stability of plane Poiseuille flow of a highly elastic liquid, J. Non-Newtonian Fluid Mech. 3 (1977) 179–195.

[18] R.G. Larson, Constitutive Equations for Polymer Melts and Solutions, Butterworths, Boston, 1988.

[19] V. Gkanis, S. Kumar, Instability of creeping Couette flow past a neo-Hookean solid, Phys. Fluids. 15 (2003) 2864–2871.

[20] L. Srivatsan, V. Kumaran, Stability of the interface between a fluid and gel, J. Phys. II. France 7 (1997) 947–963.